Crosstalk between tubulin glutamylation and tyrosination regulates kinesin-3-mediated axonal transport

Odvogmed Bayansan, Muhammad Safwan Khawaja, Dwika Sarnia Putri, and Oliver Ingvar Wagner*

National Tsing Hua University, Institute of Molecular and Cellular Biology,

Department of Life Science, Hsinchu, 30013, Taiwan (R.O.C.)

***Corresponding author**:

Dr. Oliver I. Wagner

Professor

National Tsing Hua University

Institute of Molecular and Cellular Biology & Department of Life Science

101, Sec. 2, Kuang-Fu Road, Hsinchu 30013, Taiwan (R. O. C.)

Email: owagner@life.nthu.edu.tw

Phone: +886-3-574-2487, Fax: +886-3-571-5934

Keywords: Post-translational modifications, tubulin, glutamylation, tyrosination, KIF1A, C. elegans, axonal transport

ABSTRACT

Tubulin post-translational modifications (PTMs) are critical regulators of microtubule function and diversity in neurons. In *Caenorhabditis elegans*, we investigated how tubulin deglutamylases (CCPP-1 and CCPP-6) and polyglutamylases (TTLL-5 and TTLL-9) affect kinesin-3/UNC-104–mediated axonal transport. Loss of CCPP-1 not only facilitated tubulin polyglutamylation as expected, but it also leads to increased tyrosination. Vice versa, loss of TTLL-5 reduced tubulin polyglutamylation as expected, but at the same time leads to reduced tyrosination as well. This crosstalk in tubulin PTM appears to be critical feature such as no tyrosination or detyrosination enzymes are known in in *C. elegans*. Notably, acetylation and detyrosination remained unaffected in the deglutamylation and polyglutamylation mutants. Functionally, reduced glutamylation and tyrosination improved kinesin-3 KIF1A/UNC-104 transport characteristics. Conversely, increased glutamylation and tyrosination negatively affected the movement of both UNC-104 motor and its cargo RAB-3. UNC-104 motors visibly accumulate in neuronal cell bodies of *ccpp-1* mutants while being significantly reduced in *ttll-5* mutants. In *ttll-5* mutants, motors tend to cluster along distal axonal regions and these cluster are reduced in *ccpp-1* mutants revealing a role of tubulin PYM in axonal motor scaffolding. Employing promoter fusions, we confirmed that all investigated PTM enzymes express in neurons and colocalize with UNC-104. Moreover, co-immunoprecipitation assays revealed that hyperglutamylated tubulin appears in a physical complex with UNC-104, while hypoglutamylated tubulin binds less effectively to the motor. In our model, highly negatively charged polyglutamylated tubulin traps UNC-104 onto microtubules via increased charge-interactions. Tubulin "stickiness" is reduced in polyglutamylase mutants leading to increased motor speeds. Animal behavioral assays revealed that both hyper- and hypoglutamylated tubulin mutant worms act less responsive to harsh and soft touch, highlighting *C. elegans* as a valuable model for investigating tubulin PTM-related neurological disorders.

INTRODUCTION

Axonal transport is a fundamental cellular process essential for neuronal function and survival. Two major classes of microtubule-based molecular motors drive this transport: kinesins mediate anterograde transport, while cytoplasmic dynein is responsible for retrograde transport. Axonal transport requires precise regulation through multiple mechanisms, including motor protein activation/inactivation, cargo binding specificity, and coordination between opposing motors, known as tug-of-war (Hirokawa *et al*, 2010). Disruptions in axonal transport atre linked to numerous neurodegenerative disorders including Alzheimer's disease, Parkinson's disease, amyotrophic lateral sclerosis (ALS) as well as Huntington's disease (Millecamps & Julien, 2013). Kinesin-3 KIF1A is the major axonal transporter of synaptic vesicles and is termed UNC-104 in *C. elegans*. KIFA/UNC-104 comprises a N-terminal motor domain, a regulatory neck linker, a lysine-rich K-loop, a forkhead-associated (FHA) domain, coiled-coil regions that mediate dimerization, and a C-terminal cargo-binding domain containing a pleckstrin homolog (PH) domain for membrane attachment (Siddiqui & Straube, 2017). The K-loop, a positively charged region enriched in lysine, serves as a microtubule-binding surface by interacting with the glutamate-rich and negatively charged C-terminal tails of β-tubulin (E-Hook) (Lessard *et al*, 2019; Soppina & Verhey, 2014). Mutations in the unc-104 gene results in severe paralysis of nematodes due to synaptic transmission defects (Hall & Hedgecock, 1991), and KIF1A-deficient mice die during embryonic stages due to sensory neuron degeneration (Yonekawa *et al*, 1998). Mutations in KIF1A are linked to hereditary spastic paraparesis (HSP), Charcot-Marie- Tooth (CMT) disease and KIF1A-associated neurological diseases (KAND) causing severe neurological phenotypes (Citterio *et al*, 2015; Morikawa *et al*, 2022). UNC-104 motor activity and cargo recognition are tightly regulated by synaptic scaffolding proteins Liprin-α /SYD-2 and LIN-2/CASK (Muniesh *et al*, 2020; Wagner *et al*, 2009; Wu *et al*, 2016) as well as UNC-10/Munc (Bayansan *et al*, 2025). Although microtubules are structurally conserved, they exhibit remarkable functional diversity across different cell types due the incorporation of various tubulin isotypes as well as rich post-translational modifications (PTM) (Janke & Magiera, 2020). Tubulin PTM regulates the interaction of microtubules with microtubule-associated proteins (MAPs), motor proteins, and microtubule severing enzymes (e.g., spastin) modulating microtubule

dynamics, intracellular transport and cell polarity. Mutations in tubulin isotypes result in disruption of the microtubule network during early brain development, leading to a group of neurological disorders known as tubulinopathies (Romaniello *et al*, 2015). Tubulin PTMs are mediated by enzymes, occurring either inside tubulin body (e.g., acetylation) or on the flexible C-terminal tails (e.g., glutamylation) (Janke & Magiera, 2020). Tubulin polyglutamylation involves the addition of negatively charged glutamate chains to the C-terminal tails of α- and β-tubulin by tubulin tyrosine ligase-like (TTLL) enzymes. The mammalian genome encodes nine TTLL enzymes (TTLL1, 2, 4, 5, 6, 7, 9, 11 and 13) (van Dijk *et al*, 2007) with TTLL1 and 7 abundantly expressed o neurons. TTLL1 preferably modifies α-tubulin, while TTLL7 modifies β-tubulin. TTLL1 acts to prevent degeneration of Purkinje cell degeneration (*pcd*) and myelinated axons in mice (Bodakuntla *et al*, 2021). Polyglutamylation regulates binding between kinesin motors and MAP1B, MAP2 and Tau (Bonnet *et al*, 2001) and loss of TTLL1 leads to decreased microtubule-binding affinity of KIF1A, but not KIF3A or KIF5 (Ikegami *et al*, 2007). Increased polyglutamylation is also correlated to increased microtubule severing by recruiting spastin and katanin (Lacroix *et al*, 2010; Valenstein & Roll-Mecak, 2016). The *C. elegans* genome encodes six TTLLs: TTLL-4, -5, -9, -11,-12, and -15 (Lu & Zheng, 2022). TTLL-4 is homolog to TTLL4, TTLL-5 is homolog to TTLL5, TTLL-9 is homolog to TTLL9, TTLL-11 is homolog to TTLL11, and TTLL-15 is ortholog to TTLL5 (Chawla *et al*, 2016). Polyglutamylation chains are removed by *c*ytosolic *c*arboxy*p*eptidase enzymes (CCP) (M14 metallocarboxypeptidases) (Kalinina *et al*, 2007; Rogowski *et al*, 2010). Six CCP enzymes have been identified in mammals (Berezniuk *et al*, 2013; Wu *et al*, 2015); however, only CCP1, 4, 5 and 6 reveal functional deglutamylase activity (Kimura *et al*, 2010). CCP1 removes penultimate glutamate residues from α-tubulin to produce Δ2 tubulin (Berezniuk *et al*, 2012; Hotta *et al*, 2023). While CCP1 shortens polyglutamylation chains from the C- terminus of tubulin by removing long glutamylation chains from α- and β-tubulin, CCP5 preferentially cleaves off α- and γ-linked glutamates at the branch point of tubulin (Berezniuk *et al.*, 2013; Rogowski *et al.*, 2010). Absence of CCP1 leads to hyperglutamylated tubulin resulting in neuronal degeneration, axonal swelling and perturbed axonal transport (Fernandez-Gonzalez *et al*, 2002; Gilmore-Hall *et al*, 2019; Magiera *et al*, 2018). *C. elegans* expresses only two deglutamylase enzymes, CCPP-1 and 6 (Kimura *et al.*,

2010; O'Hagan *et al*, 2011). CCPP-1 is homolog to CCP1, while CCPP-6 shares homology with CCP5 in mammals (Kimura *et al.*, 2010; O'Hagan *et al.*, 2011). In male specific neurons, loss of CCPP-1 causes defects in ciliary structure and regulates localization and motility of kinesin-3 KLP-6 and PKD-2 as well as kinesin-2 OSM-3/KIF17. Interestingly, TTLL-4 suppresses these ciliary defects in *ccpp-1* mutants (O'Hagan *et al.*, 2011). In injured *C. elegans* neurons, DLK-1 signaling controls microtubule dynamics by downregulating KLP-7 (kinesin-13) and upregulating CCPP-6. The latter enhances Δ2 modification of α-tubulin, thereby promoting microtubule growth and sustaining axon regeneration (Ghosh-Roy *et al*, 2012). Unlike CCPP-1, CCPP-6 is not essential for ciliary function, and *ccpp-1/ccpp-6* double mutants reveal no enhanced ciliary defects (Klimas *et al*, 2023). Tubulin tyrosination is catalyzed by tubulin tyrosine ligase (TTL) enzymes that add tyrosination residues to the C-terminus of detyrosinated α-tubulin (Westermann & Weber, 2003). Tyrosine can be removed by metalloprotease vasohibin (VASH1/2) in complex with small vasohibin-binding protein (SVBP) (Aillaud *et al*, 2017; Nieuwenhuis *et al*, 2017). Detyrosinated tubulin can then undergo further processing involving the removal of the final two or three C-terminal glutamate residues from α-tubulin via CCP generating (neuron specific) Δ2 and Δ3 tubulins (Paturle-Lafanechere *et al*, 1994). Tyrosinated tubulin is a marker of dynamic microtubules in growth cones and distal regions of neurites. In contrast, detyrosinated tubulin is a feature of stable microtubules in axon (Moutin *et al*, 2021). Kinesin-1 motor preferably binds to detyrosinated microtubules in axons (Dunn *et al*, 2008), while kinesin-3 and kinesin-5 preferably bind to tyrosinated tubulin (Guardia *et al*, 2016; Kahn *et al*, 2015). Absence of tubulin tyrosination enzymes induces lethal neuronal defects in mice (Erck *et al*, 2005; Pagnamenta *et al*, 2019). Interestingly, neither tyrosination nor detyrosination enzymes are expressed in *C. elegans*. Acetylation occurs at lysine 40 of α-tubulin inside the hollow microtubule body and is catalyzed by the enzyme α-tubulin acetyltransferase (αTAT) homologous to MEC-17 in *C. elegans*. This modification is prevalent in long-lived microtubules to enhance microtubule stability and resistance to mechanical stress (Li and Yang, 2015). Loss of MEC-17 leads to microtubule instability and axonal degeneration in *C. elegans* (Neumann & Hilliard, 2014).

MATERIALS AND METHODS

Worm strains and plasmid design

Worms were maintained at 20°C on NGM agar plates seeded with uranyl auxotroph OP50 *E. coli* strain according to standard methods (Brenner, 1974). Rescue strain *e1265*;*Punc-104::unc-104::mrfp* and construct design of *Punc-104::unc-104::mrfp* as well as *Punc-104::mCherry::rab-3* were described previously (Tien *et al*, 2011; Wagner *et al.*, 2009). To generate polyglutamylase mutants expressing UNC-104::mRFP, *e1265*;*Punc-104::unc-104::mRFP* male worms were crossed with either OC343 *ttll-5(tm3360)* or OC419 *ttll-9(tm3889)* hermaphrodites to generate OIW 128 *ttll-5(tm3360);nthEx[Punc-104::unc-104::mrfp]* and OIW 129 *ttll-9(tm3889);nthEx[Punc-104::unc-104::mrfp],* respectively. To generate deglutamylase mutants expressing UNC-104::mRFP, *e1265*;*Punc-104::unc-104::mrfp* male worms were crossed with either RB1522 *ccpp-1(ok1821)* or RB625 *ccpp-6(ok382)* hermaphrodites to generate OIW 130 *ccpp-1(ok1821);nthEx[Punc-104::unc-104::mrfp]* and OIW 131 *ccpp-6(ok382);nthEx[Punc-104::unc-104::mrfp]*, respectively. Double mutants were generated by crossing *ccpp-6(ok382);nthEx[Punc-104::unc-104::mrfp]* male worms with *ccpp-1(ok1821)* hermaphrodites to generate OIW 131 *ccpp-1(ok1821);ccpp-6(ok382);nthEx[Punc-104::unc-104::mrfp]* animals. For all crossings, homozygous animals were screened after backcrossing and then genotyped. For cargo motility experiment, existing plasmid *Punc-104::mCherry::rab-3* was injected at 80 ng/µl into N2, *ccpp-1(ok1821)* and *ccpp-6(ok382)* mutants to either generate OIW 131 N2;*nthEx[Punc-104::mcherry::rab-3],* OIW 132 *ccpp-1(ok1821);nthEx[Punc-104::mcherry::rab-3]* or OIW 133 *ccpp-6(ok382);nthEx[Punc-104::mcherry::rab-3]*. For transcriptional fusions, we amplified the promoter region of *ccpp-1* using forward aaaGCATGCgaagctgaaaagttg and reverse CTTCTTTACAGTATTTCAGCTGaaa to generate a 2534 bp amplicon. c*cpp-6* region was amplified using forward aaaaGCATGCtgaacgtgaaataaatc and gttttaaagtaaaagttaCAGCTGaaa reverse primers to generate a 3512 bp amplicon. The transcriptional region of *ttll-5* was amplified using forward aaaAAGCTTtttttcatcacactcgg and GAGGATTTTTGACGACGTCaaa reverse primers to generate a 2588 bp amplicon. pPD95.77 vector from Andrew Fire library was then used to generate *Pccpp-1::gfp, Pccpp-6::gfp* and *Pttll-5::gfp*. For colocalization assays, we injected either plasmid *Pccpp-1::gfp*, *Pccpp-6::gfp* or *Pttll-*

5::gfp along with *Punc-104::unc-104::mrfp* (at each 80 ng/µl) into N2 wild type worms to generate OIW 134 N2;*nthEx[Punc-104::unc-104::mrfp;Pccpp-1::gfp],* OIW 135 N2;*nthEx[Punc-104::unc-104::mrfp;Pccpp-6::gfp]* or OIW 136 N2;*nthEx[Punc-104::unc-104::mrfp; Pttll-5::gfp].*

Western blotting and Co-immunoprecipitation assays

Young adult worms (15-20 plates) were used for protein extraction, following a previously described protocol (Ward *et al*, 1988). Worms were harvested by washing the plates with 0.1M NaCl solution three times, followed by 60% sucrose flotation. Worms from the sucrose layer were collected and washed twice with cold water and 1x homogenization buffer (HB). Subsequently, 1x HB with DTT and protease inhibitor was added to the harvested worms and the sample was stored at -80°C overnight. The following day, harvested worms were subjected to French press for protein extraction. Quantification was then carried out using commercial BCA kits (Prod# 23225, Pierce ™ BCA protein kit, Thermo Scientific). For Western blotting, 100 µg of total protein was loaded per lane. Membranes were blocked with milk powder for 1 hour at room temperature. To detect polyglutamylated tubulin (PolyE), we used anti-Polyglutamylate chain (AG-25B-0030, AdipoGen, polyclonal, rabbit) antibody at 1:2000 dilutions, followed by anti-rabbit secondary antibody (GTX 213110-01) incubation at 1:4000 dilution. Tyrosinated tubulin was detected using an anti-tyrosinated tubulin antibody (T9028, Sigma, monoclonal, mouse) at 1:1000 dilutions, followed by an anti-mouse secondary antibody (GTX 213111-01) at 1: 2000 dilution. Detyrosinated tubulin was detected using anti-detyrosinated tubulin (AB3201, Sigma, polyclonal, rabbit) at 1:500 dilutions, followed by anti-rabbit secondary antibody (GTX 213110-01) at 1:1000 dilutions. Acetylated tubulin was detected using anti-acetylated tubulin T7451 (6-11B-1, Thermo Fisher, monoclonal, rabbit) at 1: 500 dilutions, followed by anti-rabbit secondary antibody (GTX 213110-01) incubation at 1:1000 dilutions. Anti-GAPDH antibody (GTX100118, GeneTex, polyclonal, rabbit) at 1:2500 dilutions, followed by anti-rabbit secondary antibody (GTX 213110-01) incubation at 1:5000 dilution was used as positive control. Primary antibodies were incubated at 4°C overnight while secondary antibodies were incubated at room temperature for 4 hours. To detect lower molecular weight proteins, we used a 12% SDS-PAGE gel with 30% acrylamide, while for

higher molecular weight proteins, a 6% SDS-PAGE gel with 40% acrylamide was used. For co-immuno-precipitation (Co-IP) assays, 1 mg protein extract incubated with 50 µl protein G beads (CAT# LSKMAGG10, Millipore) and 5 µg UNC-104 antibody (GeneTex, commissioned by us, detects a N-terminal epitope, polyclonal, rabbit). After overnight incubation, worm lysates were subjected to Western blotting using polyglutamylated antibody (PolyE) to detect polyglutamylated tubulin bound to UNC-104. Antibody dilutions and incubation times were identical to those described for Western blot assays. All band intensity measurements were performed using NIH ImageJ software, following a published protocol (Schneider *et al*, 2012).

Motility and motor clustering analysis

Worms were immobilized on 2% agarose-coated cover slides along with 7 µl of M9 buffer for motility and motor clustering analysis experiments. No anesthetics such as Levamisole was used. An Olympus IX81 microscope with a DSU Nipkow spinning disk unit connected to an Andor iXon DV897 EMCCD camera was employed for high-resolution and high-speed time-lapse imaging at 4-5 frames per second. Time-lapse images from a selected area were captured and then converted to kymographs using imaging analysis software NIH ImageJ. The “straighten plugin” was used to straighten curved axons and the “reslice” and “stack” plugins were used to generate kymographs (Suppl. Fig. S1B). A pause is defined if motors or cargo move less than 0.07 µm/s, and each calculated velocity event does not contain any pauses. A moving event is defined as a single motility occurrence typically right after a pause or a reversal, and such an event ends when the motor again pauses or reverses (Suppl. Fig. S1C). For motor clustering analysis, ALM neurons were divided into four regions: cell body, initial, middle and distal regions as shown in Suppl. Fig. S1D. Number of particles in cell bodies were counted manually by visual inspection. For axonal regions, the NIH ImageJ "analyze particles" plugin was used to quantify the number of clusters in axons. After straightening the image, the threshold was adjusted and following parameters applied: distance in pixels = 1, known distance = 0.159, pixel aspect ratio = 1, and unit of length = µm. Travel distances of UNC-104 clusters from axon hillock to initial region was measured using the NIH ImageJ "line tool" after straightening the neuron and applying the same parameters (Figs. 6F, 8C). Density of UNC-104 clusters was calculated by

dividing the number of particles in different regions of the axons by 10 µm (Figs. 6E, 8B). PMUV (Persistent Movement at Uniform Velocity) refers to how long a motor continues to move at a constant speed (Figs. 6C+7G). For correlation analysis in Fig. 8D-G, r-values were calculated within two selected datasets (x = velocity, y = distance) using Pearson's correlation coefficient and unpaired, two-tailed Student's t-test to determine the p values.

Confocal imaging

Worms were immobilized on 2% agarose pads with 7 µl of M9 and covered with a cover slide for imaging. No anesthetics such as Levamisole was used. A Zeiss LSM780 confocal laser scanning microscope was employed for fluorescent imaging (Fig. 9, Suppl. Fig. S2). To measure colocalization between UNC-104 and promoter fusions of genes encoding PTM enzymes, we employed both Mander's (MOC) and Pearson's (PCC) correlation coefficients. MOC ranges between 0 to 1 and PCC ranges between -1 and 1. MOC measures the co-occurrence or overlap of two signals, based on absolute pixel intensities. PCC determines the linear correlation between pixel intensities, independent of absolute intensity values. The NIH ImageJ "polygonal selection tool" was selected to determine the region of interest (ROI) in an image. After background subtraction, NIH ImageJ "intensity correlation analysis" plugin was used to generate either MOC or PCC. PDM images refer to the product of the differences from the mean of red and green fluorescence intensities. It is calculated as: (red intensity – mean red intensity) × (green intensity – mean green intensity).

Whole-mount immunostaining

Young adult *e1265*;Punc-104::UNC-104::GFP rescue worms were synchronized, washed with M9 buffer, and collected in 2 ml Eppendorf tubes. Worms were then fixed with 1 ml of 4% paraformaldehyde and subjected to three cycles of freeze-thawing in liquid nitrogen, each lasting 3 minutes. After the final freeze cycle, worms were incubated in 4% paraformaldehyde at 4°C overnight. The following day, worms were washed with PBST and incubated with 1 ml of β-mercaptoethanol at 37°C overnight. After incubation, worms were washed again with PBST and treated with 500 µl of collagenase (Cat# C0773, Sigma) at 37°C for 6.5 hours. Worms were then blocked for 1 hour at room temperature. Afterwards, worms were washed

with antibody buffer and incubated with primary antibodies (either anti-Polyglutamylated tubulin PolyE or anti-tyrosinated tubulin) at 1:200 dilutions (4°C overnight). Subsequently, worms were incubated with secondary antibodies (anti-rabbit ab150119 or anti-mouse A-11005) at 1:500 dilutions (4 hours at room temperature). Worms then washed thrice with antibody buffer, with each washing lasting 15 min. Afterwards, worms were mounted on a microscope slide and subjected to imaging.

Harsh and soft touch responses

To investigate physiological consequences of the mutations, we use N2 and mutant worms at young adult stage. Both soft and harsh touch assays were performed to assess touch responses. For the soft touch assay, an eyelash was used to gently strike the worm laterally at the mid-body region. In contrast, a platinum wire was used for the harsh touch assay, applying a stronger stimulus to the same area. Each worm was tested four times per assay. A positive response was defined as a clear backward movement following the stimulus (MEC response). Worms that responded as expected all four times were scored as 100%, indicating full responsiveness.

Statistics

To determine whether acquired data follow a Gaussian distribution or not, we plotted histograms. If Gaussian distribution was present, we used ordinary one-way ANOVA with Dunnett's test for multiple comparisons or unpaired Student's t-test for two-group comparisons. For non-Gaussian distributions, we used either (non-parametric) Kruskal-Wallis one-way ANOVA Dunn's test for multiple comparisons, or unpaired Mann-Whitney test for two-group comparisons. For Western blot and Co-IP data analyses we used either one-way ANOVA with Dunnett's test for multiple comparisons, or unpaired two-tailed Student's t-test for two-group comparisons. Box-and-whisker plots display the maximum, upper quartile, median, lower quartile, and minimum values.

RESULTS

CCPP-1, but not CCPP-6, cleaves polyglutamylated tubulin

To investigate the effects of ccpp-1 and ccpp-6 mutations on tubulin glutamylation, we employed anti-polyglutamylated tubulin PolyE antibody, which detects longer than four polyglutamylated chains. It has been reported that deglutamylase CCP1 in mammals shortens tubulin polyglutamylation by removing long polyglutamylated tubulin chains from α- and β-tubulin (Berezniuk *et al.*, 2012). To examine whether a similar function exists for CCPP-1 in *C. elegans*, we conducted Western blots, using strain RB1522 *ccpp-1(ok1821)* that carries a 1770 bp deletion in putative 5′ regulatory sequences and the first 5 exons of the *ccpp-1* gene, resulting in a null mutant (O'Hagan *et al.*, 2011) (Fig.1 A). We reveal that the level of poly-glutamylated tubulin chains in *ccpp-1(ok1821)* was significantly elevated compared to wild type and *ccpp-6(ok382)* mutants (Fig. 1B-D), consistent with the known activity of CCP1 in mammals. In *C. elegans*, CCPP-6 is the homolog of mammalian CCP5 and unlike CCP1, it specifically removes the branching-point glutamate — the first glutamate directly linked to the γ-carboxyl group of the glutamate residue in the tubulin backbone (Berezniuk *et al.*, 2013). To investigate the function of CCPP-6, we use strain RB625 *ccpp-6(ok382)* that carries a 532 bp deletion removing the start codon of the gene as well as the first two exons (Dominguez *et al*, 2022) (Fig.1A). From Figure 1B it is obvious that in *ccpp-6(ok382)* mutants, the level of polyglutamylated tubulin remains unaffected in *ccpp-6* mutants(Fig. 1B+C, E). Also, here we may argue with a compensatory function: if CCPP-6 is mutated (or downregulated), CCPP-1 may be upregulated. That compensatory pathways may exist shows a double mutant experiment in Figure 1C: while *ccpp-6* shows no phenotype, the double mutant shows an enhanced ccpp-1 phenotype (Fig.1 B+C, F) pointing to synthetic interactions in parallel (and partial redundant) pathways.. Interestingly, a study by Klimas et al. shows that deletion of both CCPP-1 and CCPP-6 deglutamylases did not enhance the ciliary phenotype of the single *ccpp-1(ok1821)* mutation also suggesting linear epistatic pathways (Klimas *et al.*, 2023).

TTLL-5 works as a polyglutamylation initiator in C. elegans

TTLL enzymes are classified as initiators or elongators based on their enzymatic activity during the polyglutamylation process. In mammals, TTLL4 and TTLL7 initiate polyglutamylation by adding the first

glutamate residue to the γ-carboxyl group of a glutamate in the tubulin C-terminal tail, establishing the branching point of the side chain. In contrast, TTLL1, TTLL6, and TTLL11 all function as elongators, extending that chain by adding additional glutamate residues (van Dijk *et al.*, 2007). Dysregulation of TTLL enzymes has been linked to various pathologies, including neurodegeneration and cancer, highlighting the importance of balanced polyglutamylation in cellular homeostasis (Kashiwaya *et al*, 2010; Ping *et al*, 2023). To find the initiator among the TTLL enzymes in worms, we utilized two mutant strains: OC343 *ttll-5*(*tm3360*) and OC419 *ttll-9*(*tm3889*). The *ttll-5*(*tm3360*) allele contains an 833 bp deletion and a 10 bp insertion, while *ttll-9*(*tm3889*) carries a 509 bp deletion along with a 43 bp insertion. Both mutations introduce frameshifts that are predicted to produce nonfunctional proteins due to premature stop codons (Fig. 2A). Western blot analyses revealed that in *ttll-5* mutants, the levels of polyglutamylated tubulin were significantly reduced compared to wild type control (Fig. 2B-D). These results are as expected due to loss of a polyglutamylase enzyme. In contrast, *ttll-9* mutants did not show any noticeable change in polyglutamylation levels (Fig. 2B+C, E), suggesting that TTLL-9 may not be essential for initiating polyglutamate chains under normal conditions. These findings indicate that TTLL-5 plays a major role in initiating polyglutamylation in *C. elegans*.

Crosstalk between tubulin glutamylation and tyrosination

Microtubules are subject to a variety of post-translational modifications (PTMs), which regulate their stability and interactions with motor proteins (Janke & Magiera, 2020). Emerging evidence suggests complex crosstalk between polyglutamylation, detyrosination, and acetylation, indicating that these modifications do not work independently but rather influence each other's dynamics and cellular outcomes (Ebberink *et al*, 2023; Genova *et al*, 2023; Mahalingan *et al*, 2020). To explore the interrelationship between these PTMs, we examined the extent tyrosinated, detyrosinated, and acetylated tubulin in both deglutamylase (*ccpp-1* and *ccpp-6*) and polyglutamylase (*ttll-5* and *ttll-9*) mutants in *C. elegans*. Western blot analysis revealed that tyrosinated tubulin levels were significantly elevated only in *ccpp-1*, however, remaining unchanged in both *ccpp-6* single or in *ccpp-1*;*ccpp-6* double mutants (Fig. 3A+B, E-G). These data suggest that ccpp-6 acts antagonistically or in a compensatory pathway that suppresses the *ccpp-1* mutant phenotype.

In contrast, detyrosinated tubulin levels remain unchanged across single and double mutants (Fig. 3C-G), suggesting a selective effect of deglutamylation on tyrosination but not detyrosination. Intriguingly, tyrosinated tubulin levels were significantly decreased in both *ttll-5*(*tm3360*) and *ttll-9*(*tm3889*) mutants compared to wild type (Fig. 4A+B, E+F), whereas detyrosinated tubulin levels remain unchanged in these strains (Fig. 4C-E, F). As above shown (Fig. 1C), *ccpp-1(ok1821)* mutants exhibited hyperglutamylated tubulin, accompanied by elevated tyrosinated tubulin levels (Fig. 3B), while *ttll-5(tm3360)* mutants showed reduced polyglutamylation (Fig. 2C+E) along with decreased tyrosinated tubulin levels (Fig. 4B). These data suggest a potential regulatory link in which hyperglutamylation promotes tyrosination of tubulin, whereas hypoglutamylation leads to reduction in tyrosination though no tyrosination enzymes are known in nematodes. To further explore the relationship between polyglutamylation and other PTMs, we also assessed acetylated tubulin levels. However, no significant changes were observed in either deglutamylase or polyglutamylase mutants (Fig. 5), suggesting no crosstalk between polyglutamylation and acetylation. Together, these findings indicate that polyglutamylation selectively regulates the tyrosination state of tubulin, but not its acetylation or detyrosination. This highlights an important functional PTM crosstalk that may fine-tune microtubule dynamics and motor protein interactions.

Hypoglutamylated tubulin positively affects UNC-104 transport

To determine the functional consequences of this PTM cross talk on axonal transport, we assessed the motility of UNC-104, tagged with monomeric red fluorescent protein (mRFP). This fluorescent tag was selected for its low self-aggregation properties, allowing clearer visualization of motor movement in live animals without artificial aggregation (Eves-van den Akker *et al*, 2014; Hamed *et al*, 2018; Kimura *et al*, 2007; Wang *et al*, 2019). UNC-104(KIF1A) is the major transporter of synaptic vesicles in neurons, and we specifically focus on the ALM (Anterior Lateral Mechanosensory) neuron, spreading nearly 50% of the worm's body to allow for observation of long-range axonal transport (Suppl. Fig. S1A). As shown in Fig. 2, *ttll-5(tm3360)* mutants display reduced levels of polyglutamylated tubulin, indicating hypoglutamylation as expected for a polyglutamylase knockout. Our motility analysis revealed that both anterograde velocity and run length of UNC-104 were significantly increased in both *ttll-5(tm3360)* and *ttll-9(tm3889)* mutants

(Fig. 6A+B). To support these findings, UNC-104's persistent movement in the anterograde direction—indicating how far the motor can travel without detaching from the microtubule—was significantly increased in both polyglutamylase mutants (Fig. 6C). These results show that reduction in tubulin polyglutamylation enhances the motility of kinesin-3 along axonal microtubules. At the same time, density of UNC-104 clusters per 10 µm increased in regions of the axon in both polyglutamylase mutants compared to wild type (Fig. 6D+E). Consequently, density of UNC-104's cluster in cell bodies decreased in *ttll-5(tm3360)* mutants (Fig. 6D+E) in accordance to enhanced transport rates in both polyglutamylase mutants. Moreover, UNC-104 travel distances are significantly increased in *ttll-9(tm3889)* mutants - once more pointing to facilitated transport (note that in *ttll-5(tm3360)* travel distances are comparable to wt though, Fig. 6F). Noteworthy is also that in *ttll-5(tm3360)* mutants clusters become more diffused suggesting reduced motor scaffolding in these mutants. To summarize, these results provide functional evidence that polyglutamylation levels effectively modulate axonal transport.

Hyperglutamylated tubulin negatively affects kinesin-3 transport

Since hypoglutamylated tubulin enhances motility of UNC-104, we then investigated the effect of hyperglutamylation on axonal transport. As shown in Fig. 7A, loss of deglutamylases CCPP-1 and CCPP-6 led to a significant reduction in anterograde velocities of UNC-104. Double mutants further elevated this effect pointing to parallel (and partial redundant) pathways. Interestingly, anterograde run lengths of UNC-104 remain unchanged in single mutants and only the double mutant reflects significant changes once more consistent with a synthetic phenotype. Though UNC-104 is an anterograde motor and does not inherit the intrinsic ability to move retrogradely, it is interesting to further analyze retrograde features (likely based on the interaction with the retrograde motor dynein). Indeed, direct interactions between UNC-104 and dynein have been reported (Chen *et al*, 2019) leading to tug-of-war events and eventually passive retrograde displacements of UNC-104. In terms of retrograde velocities of UNC-104, we found a significant decrease in single and double deglutamylase mutants (Fig. 7C). Similarly, retrograde run lengths of UNC-104 were significantly decreased in single *ccpp-6* and double mutants (Fig. 7D). It is interesting to see that for this feature (passive retrograde motility of UNC-104) the double mutant mostly phenocopies ccpp-6 assuming

linear epistasis in which CCPP-6 is downstream of CCPP-1. Furthermore, increasing directional changes (motor reversals) reflect increased interactions between UNC-104 and dynein (Fig. 7E). Also, the fact that UNC-104 pausing per 10 µm was increased (Fig. 7F) is as expected for measured decreased velocities in both directions (Fig. 7A+C). However, UNC-104's persistent movement remains unchanged in deglutamylase mutants (Fig. 7G). We then examined motility of UNC-104's major cargo RAB-3 tagged with mCherry. It is expected that motility of the major cargo alone should be comparable to the motility of its major transporter (UNC-104) alone. Indeed, loss of CCPP-1 and CCPP-6 lead to significant reductions in both anterograde velocities as well as run lengths of RAB-3 (Fig. 7H+I). Similarly, retrograde velocity (except for *ccpp-1*) and run lengths of RAB-3 were significantly decreased (Fig. 7J+K). These results suggest that hyperglutamylation perturbs the whole transport complex (motor + cargo).

Effect of deglutamylase enzymes on UNC-104 axonal cluster patterns

We previously reported that UNC-104 tends to form dynamic cluster along the lengthy ALM neuron generated by scaffolding protein SYD-2 (Wagner *et al.*, 2009). Changes in these cluster patterns, and analysis of distal distance cluster to the initial axonal segment, provides insight into the quality of axonal transport and therefore the physiological impact of neurons. Indeed, it has been reported that in a *pcd* (Purkinje cell degeneration) mouse with a CCP1 mutation severe neurodegenerative phenotypes are generated with impaired axonal transport consistent with our results in Figure 7 (Fernandez-Gonzalez *et al.*, 2002; Li *et al*, 2020). Therefore, we analyzed changes in UNC-104 axonal cluster patterns to investigate the physiological effects of CCPP-1 and CCPP-6 in *C. elegans* neurons. Specifically, we determined size and spatial distribution of UNC-104 clustering along the axon as well as their distances from the axon hillock to distal regions (reflecting UNC-104's travel distances). For a more in-depth analysis, we divided the ALM neuron into 4 sections: cell body, initial-, middle- and distal regions (Suppl. Fig. S1D). As a result, in wild types, motor clusters were distributed in a gradient with more cluster in proximal and less clusters in distal regions (Fig. 8A+B). Loss of CCPP-1, however, increased density of clusters in cell bodies with a concomitantly visible decrease in distal axonal regions (Fig. 8A+B). This motor retention in cell bodies led to significant reductions in travel distances in *ccpp-1(ok1821)* mutants and double mutants (Fig. 8C). Interestingly, the

effect of cluster retention was not as severe in *ccpp-6* mutants and no changes in travel distances were determined (Fig. 8B+C). In fact, the double mutant seems to phenocopy the effects of ccpp-1 alone pointing to linear epistasis with CCPP-1 downstream of CCPP-6. We then wondered if correlations exist between motor speeds (Fig. 7A) and travel distances (Fig. 8C). Indeed, a strong positive correlation between motor speeds and travel distances across all single and double deglutamylase mutants was determined (Fig. 8D-G).

Colocalization between glutamylase enzymes and UNC-104

Above, we revealed direct effects of CCPP and TTLL enzymes on the quality of axonal transport in ALM neurons. To understand whether these effects might result from closer interactions between these enzymes and UNC-104, we cloned transcriptional fusions of CCPP-1, CCPP-6 and TTLL-5 and co-expressed them with UNC-104::mRFP in *C. elegans*. As shown in Figure 9A, transcriptional GFP reporter of CCPP-1 clearly expresses in various nerve ring neurons, ALM, tail neurons as well as male in sensory neurons. In addition, UNC-104 clearly and strongly colocalizes with the promoter fusions as shown by Mander's and Pearson's coefficients (Fig. 9C+D). On the other hand, the transcriptional GFP reporter of CCPP-6 expressed only weakly in sublaterals and dorsal axons with more clear expression in cell bodies of these neurons (Fig. 9B). Similarly, expression of GFP reporter of CCPP-6 in the nerve ring was restricted to few neurons and in ALM more pronounced in cell bodies than in axons (similar for tail neurons) (Fig. 9B). Also, colocalization with between UNC-104 and the CCPP-6 reporter fusion was less pronounced compared to UNC-104 and CCPP-1 (Fig. 9E+F). We also examined the expression pattern of a transcriptional TTLL-5 fusion in *C. elegans* (Fig. 9G) and found expression in head sensory neurons, dorsal and ventral nerve cords as well as in the epidermis. Also, for this enzyme colocalization with UNC-104 is present, however, rather weak (Fig.9I+L). It may be that used microscopic techniques are not sufficient to detect small expression levels of CCPP-6 and TTLL-5 promoter fusions, till it is intriguing that UNC-104 and CCPP-1 show such significant colocalization and co-expression patterns. We then conducted whole mount immunostaining using UNC-104::GFP wild type worms and stained them with anti-polyglu-

tamylated tubulin and anti-tyrosinated tubulin antibodies (Suppl. Fig. S2A+B). Though it turned out technically challenging to perform whole mount immunostainings, we revealed that polyglutamylated tubulin colocalized with UNC-104 in select head sensory neurons (Suppl. Fig. S2B). More critically, tyrosinated tubulin was clearly seen in *C. elegans* body neurons (including ALM) partially colocalizing with UNC-104 (Suppl. Fig. S2C).

Polyglutamylated tubulin directly interacts with kinesin-3

Based on above results revealing functional relations between UNC-104 motility and glutamylation, we wonder if polyglutamylated tubulin directly interacts with UNC-104 and whether such interactions would change in *ccpp-1* and *ttll-5* mutants. Therefore, we performed co-immunoprecipitation (Co-IP) assays to first precipitate UNC-104 (using a commissioned anti-UNC-104 antibody) and then to detect PolyE tubulin employing lysates of worms carrying *ttll-5* and *ccpp-1* alleles. As a result, in *ttll-5(tm3360)* mutants where polyglutamylated tubulin levels were significantly reduced, we also observed reduced binding of PolyE tubulin to UNC-104 (Fig. 10A-D). Conversely, in *ccpp-1(ok1821)* mutants, where polyglutamylated tubulin is elevated due to the deglutamylase knockout, polyglutamylated tubulin binding to UNC-104 significantly increased (Fig. 10E–G). Together, these findings demonstrate that polyglutamylated tubulin directly interacts with UNC-104 and that the presence or absence of glutamylation enzymes significantly regulates this interaction. To investigate potential defects in mechanosensory neurons (including ALM) upon changes in tubulin glutamylation, we performed both soft and harsh touch behavioral assays. As a result, touch responses were significantly reduced in both hypoglutamylated and hyperglutamylated tubulin mutants (Fig. 11).

These results suggest that *C. elegans* can serve as a useful model organism for studying the role of tubulin glutamylation and associated neurological diseases.

Model summarizing this study

In our model (Fig. 12), we propose that increased polyglutamylation traps kinesin-3 motors along the microtubule based on charge interactions: polyglutamylated tubulin is strongly negatively charged (Janke *et al*, 2008) that increasingly interacts with the positively charged K-Loop in the motor domain of UNC-

104 (Fig. 12C) (Benoit *et al*, 2024; Soppina & Verhey, 2014) leading to UNC-104 immobilization. However, in microtubules with more hypoglutamylated tubulin (Fig. 12B) this tubulin "stickiness" is reduced, and motors are able to move more freely. Though not shown here, increased tyrosination and hyperglutamylated microtubules may decrease microtubule stability leading to less efficient axonal transport.

DISCUSSION

Genetic pathways of ccpp-1 and ccpp-6 in C. elegans

Microtubules are highly dynamic cytoskeletal elements that undergo continuous assembly and disassembly, playing essential roles in intracellular transport, cell polarity and cell shape (van der Vaart *et al*, 2009). Microtubule dynamics are influenced by intrinsic factors such as tubulin isoforms, various PTMs, and MAPs, as well as extrinsic factors including microtubule-interfering drugs and temperature (Borys *et al*, 2020). *C. elegans* possesses only two deglutamylase enzymes: CCPP-1 and CCPP-6. As shown in Fig. 1B+C, the level of polyglutamylated tubulin was elevated in *ccpp-1(ok1821)* mutants and further increased in the double mutants.. An enhanced phenotype of one gene in double mutants (while there is no phenotype for the other gene) (Fig. 1C) often points to parallel and partial redundant pathways.. Consistenly, in a study investigating the effects of CCPP-1 and CCPP-6 on *C. elegans* cilia development the authors conclude no redundancy of CCPP-6 (Klimas *et al.*, 2023). In a study using mouse, deletion of CCP1 leads to hyperglutamylation in the cerebellum as expected, but led to a *pcd* (Purkinje cell degeneration) mouse phenotype (Fernandez-Gonzalez *et al.*, 2002; Rogowski *et al.*, 2010). On the other hand, loss of CCP6 caused hyperglutamylation only restricted to specific brain regions and did not produce a *pcd* phenotype (Kalinina *et al.*, 2007). Notably, simultaneous deletion of both CCP enzymes induces widespread hyperglutamylation and neuronal degeneration throughout the mouse brain, including in regions that remain unaffected in *pcd* mice, such as the pyramidal neurons of the cerebral cortex (Magiera *et al.*, 2018). This evidence supports that both CCP1 and CCP6 indeed function as deglutamylases but work in distinct ways. Redundancy might also explain the differing effects of CCPP-1 and CCPP-6 on UNC-104 cluster density patterns (Fig. 8A+B): while we observe a cell body retention effect for ccpp-1, movement of particles to the initial part is enhanced in ccpp-6. Nevertheless, particle distances from the axon hillock to further distal regions is decreased only

in ccpp-1, but no effects can be seen for ccpp-6. Here, once more, the double mutant phenocopies ccpp-1 suggesting a upstream role of ccpp-6 in nematodes. In summary, from the literature and our experiments we conclude partial redundancy for genes ccpp-1 and ccpp-6.

Regulation of UNC-104 motility and cargo transport efficiency by tubulin hyperglutamylation

We have clearly shown that in deglutamylase mutants, tubulin is hyperglutamylated (Fig. 1) that concomitantly leads to a reduction in UNC-104 motility (Fig. 7A+B) as well as cargo transport efficiencies (Fig. 7H+I). Vice versa, in polyglutamylase mutants, tubulin is hypoglutamylated (Fig. 2) significantly increasing motor motility (Fig. 6A-C). These findings are consistent with a study in which polyglutamylation decreases kinesin-3/KIF1A run length by 34% and landing rates by 94% using single molecule *in vitro* assays (Lessard *et al.*, 2019). Likewise, another group found that in *Ccp1*$^{-/-}$*Ccp6*$^{-/-}$ mice (with hyperglutamylated tubulin) kinesin-1-based mitochondria transport is perturbed in neurons leading to neuronal degeneration (Magiera *et al.*, 2018). To explain the impaired UNC-104 motility by hyperglutamylation (Figs. 7+8), we propose that motors are increasingly immobilized on microtubules due to increased negative surface charges upon tubulin hyperglutamylation. Indeed, it has been well documented that kinesin-3 KIF1A binds to microtubules via its positively charged K-loop (in the motor domain) that charge-interacts with the negatively charged C-terminal E-Hooks of β-tubulin (Benoit *et al.*, 2024; Zaniewski & Hancock, 2023). In our model in Figure 11, increased "stickiness" of microtubules due to hyperglutamylation increasingly traps motors on the microtubule surface. It has been also documented that hyperglutamylated tubulin destabilizes microtubules in various ways: promoting binding of microtubule severing enzymes, disrupting MAP binding and increasing microtubule catastrophe. Indeed, also *C. elegans* possesses severing proteins such as a spastin homolog SPAS-1 (Matsushita-Ishiodori *et al*, 2007), as well as katanin homologs encoded by mei-1 and mei-2 (Lu *et al*, 2004). In more detail, long polyglutamylated side chains enhance spastin- and katanin-mediated microtubule disassembly (Lacroix *et al.*, 2010), C-terminal tails of microtubules specifically bind MAP2 and Tau proteins (Boucher *et al*, 1994; Paschal *et al*, 1989) and higher levels of negatively charged polyglutamylation induces strong electrostatic repulsion that reduces MAP affinity. That polyglutamylation increases catastrophe and decreases microtubule growth has been clearly shown by other as well

(Chen & Roll-Mecak, 2023). Based on this literature evidence, we conclude that especially our observation of reduced UNC-104 clustering along axons (Fig. 8A+B) might be reflected by a disintegrated microtubule network. In summary, excessive polyglutamylation increasingly immobilizes UNC-104 based on "charge-trapping" as well as destabilizes microtubules both leading to trafficking defects causing adverse physiological effects. Particularly susceptible in neurons, where fast and precisely regulated transport is critical for proper cellular function and neuronal health. Indeed, our behavioral assays revealed that touch response decreased in both hypo- and hyperglutamylated tubulin mutants (Fig. 11) which is consistent with findings that tubulin hyperglutamylation is associated with neurodegeneration (Magiera *et al.*, 2018). Thus, *C. elegans* can be used as a model to investigate tubulin glutamylation linked to neurological diseases. Moreover, it has been shown that increased tyrosination decreases microtubule dynamic (Sanyal *et al*, 2023) that might additionally negatively affect axonal transport in *ccpp-1* mutants due to higher levels of tyrosinated tubulin (Fig. 3A+B).

Impact of hypoglutamylation on UNC-104 motility

While tubulin hyperglutamylation can be efficiently induced in deglutamylase mutants, hypoglutamylated tubulin can be well induced in polyglutamylase mutants. We have clearly shown that tubulin glutamylation is significantly reduced in *ttll-5(tm3360)* mutants (Fig. 2B+C*)*. TTLL-5 in *C. elegans* is homologous to mammalian TTLL5 (Chawla *et al.*, 2016), which polyglutamylates both α- and β-tubulin, with a preference for α-tubulin. TTLL5 is also capable of initiating and elongating polyglutamylation chains in mammals (van Dijk *et al.*, 2007). Although TTLL-9 in *C. elegans* is homologous to mammalian TTLL9 (Chawla *et al.*, 2016) and has polyglutamylase activity, it is known that TTLL9 requires interaction with other proteins to acquire enzymatic activity, due to the absence of essential domains (similar to TTLL1 and TTLL2) (Janke *et al*, 2005). This might explain that simply deleting *ttll-9* alone in *C. elegans* does not cause significant effects on tubulin polyglutamylation (Fig. 2B+C). Nevertheless, hypoglutamylation clearly enhanced UNC-104 motility (Fig. 6A-C) with concomitant increased density of motor cluster in distal regions of axons (Fig. 6D+E). These results suggest that while hyperglutamylation negatively affects UNC-104 motility, hypoglutamylation positively affects UNC-104 motility. Notably, one study shows that

hypoglutamylation induced by a TTLL1 deletion results in a twofold increase in mitochondrial motility driven by kinesin-1 (Bodakuntla *et al.*, 2021).

Crosstalk between different post-translation modifications

Microtubules encounter a wide range of PTMs that regulate their structure and function (Janke & Magiera, 2020). Specifically in dendrites, tubulin PTM largely varies: at the dendritic core, microtubules are usually more acetylated with low levels of tyrosination while microtubules at the dendritic periphery are more tyrosinated and less acetylated (Tas *et al*, 2017). Recent findings have demonstrated that vasohibin/SVBP, the enzyme complex responsible for detyrosination, shows markedly reduced activity in the absence of polyglutamylation (Ebberink *et al.*, 2023). Similarly, polyglutamylase TTLL6 revealed no activity on unmodified tubulin but 20-fold higher activity on detyrosinated tubulin (Mahalingan *et al.*, 2020). Moreover, the absence of TTLL1 and TTLL7 in *Ttll1* $^{-/-}$ *Ttll7* $^{-/-}$ double mutant mice led to high levels of acetylated tubulin (Genova *et al.*, 2023). These findings indicate potential crosstalk between polyglutamylation and other tubulin modifications, including detyrosination and acetylation. Indeed, in *ccpp-1* mutants we not only revealed tubulin hyperglutamylation (Fig. 1B+C) but also significantly increased levels of tyrosinated tubulin (Fig 3A+B). Vice versa, deletion of *ttll-5* led not only to hypoglutamylated tubulin (Fig. 2B+C) but also to reduced levels of tyrosinated tubulin (Fig 4A+B). Interestingly, detyrosinated and acetylated tubulin remain unchanged in *ccpp-1(ok1821)* and *ttll-5(tm3360)* mutants (Figs. 3C+D, 4C+D and 5A-D). Our finding of unaffected acetylation is consistent with a previous study reporting no effect on tubulin acetylation following deletions of *TTLL1* and *TTLL9* in Tetrahymena microtubules (Wloga *et al*, 2008). Because to date no tyrosination enzymes have been identified in *C. elegans*, we propose that cross talk between tubulin hyperglutamylation and hypoglutamylation regulates tubulin tyrosination via unknown additional factors in nematodes.

Tubulin tyrosination and its effect on kinesin-3 motility

As mentioned above, kinesin motors "walk" along microtubules by interacting with the C-terminal tails (CTTs) of α- and β-tubulin subunits (Benoit *et al.*, 2024; Lessard *et al.*, 2019). These CTTs are hotspots for PTMs such as tyrosination, detyrosination, acetylation, and polyglutamylation, and these modifications

clearly alter the electrostatic and steric environment of the microtubule surface (Janke & Magiera, 2020). Indeed, kinesin motors of the various classes exhibit preferences for specific tubulin modifications. For instance, in mammals, kinesin-3 and kinesin-5 preferentially bind to tyrosinated tubulin enriched on dynamic microtubules near growth cones, distal dendrites and in neuronal cell bodies (Guardia *et al.*, 2016; Kahn *et al.*, 2015). Axonal microtubules, however, are generally enriched in stable forms of tubulin such as acetylated and detyrosinated tubulin and only the very distal regions near the dynamic growth cones contain more tyrosinated tubulin (Ahmad *et al*, 1993; Nirschl *et al*, 2016). Therefore, our finding that reduced tyrosination leads to increased motor motility (Fig. 4A+B and Fig. 6A-C) does not necessarily contrast findings from others that kinesin-3 prefers tyrosinated tubulin since our observations are carried out in more proximal regions of axons as opposed to growth cones or inside neuronal cell bodies. Note that tyrosination does not affect microtubule surface charge (Szczesna *et al*, 2022), thus it is the increased polyglutamylation that predominantly affects microtubule surface charge (Fig.12).

Direct interactions between UNC-104 and PolyE tubulin regulated by hypo- and hyperglutamylation

Polyglutamylated tubulin is particularly enriched in the B-tubule of motile cilia and flagella (Lechtreck & Geimer, 2000; Orbach & Howard, 2019), where it plays a key role in regulating dynein activity and ciliary beating (Kubo *et al*, 2010; Suryavanshi *et al*, 2010). In *C. elegans,* deglutamylase (CCPP) and polyglutamylase (TTLL) enzymes are also known to be expressed in non-motile cilia and present in ciliated neurons such as head, amphid and male neurons (Chawla *et al.*, 2016; Kimura *et al.*, 2007; O'Hagan *et al.*, 2011). Interestingly, we show expression (especially of ccpp-1) also in non-ciliated neurons such as in ALM and sublaterals (Fig. 9A). More importantly, ccpp-1 promoter reporters significantly colocalize with UNC-104 (Fig. 9C+D). Strikingly, in Co-IP experiments, *ccpp-1* and *ttll-5* mutants directly regulate the amount of PolyE tubulin bound to UNC-104 (Fig. 10). These data underscore our model (Fig. 12) in which tubulin increasingly binds to UNC-104 upon hyperglutamylation (likely due to increased charge-interactions).

ACKNOWLEDGEMENTS

We acknowledge the National Bio-Resource Project (Japan) for kindly providing various strains used in this study. This work was funded by the National Science Council (now NSTC, National Science and Technology Council) under grant number NSC 107-2311-B-007-003-.

AUTHORS' CONTRIBUTIONS

OB performed experiments, analyzed data, and wrote the manuscript. MSK and DSP performed experiments and analyzed data. OIW designed experiments, obtained grants, and wrote the manuscript.

FIGURES

FIGURE 1

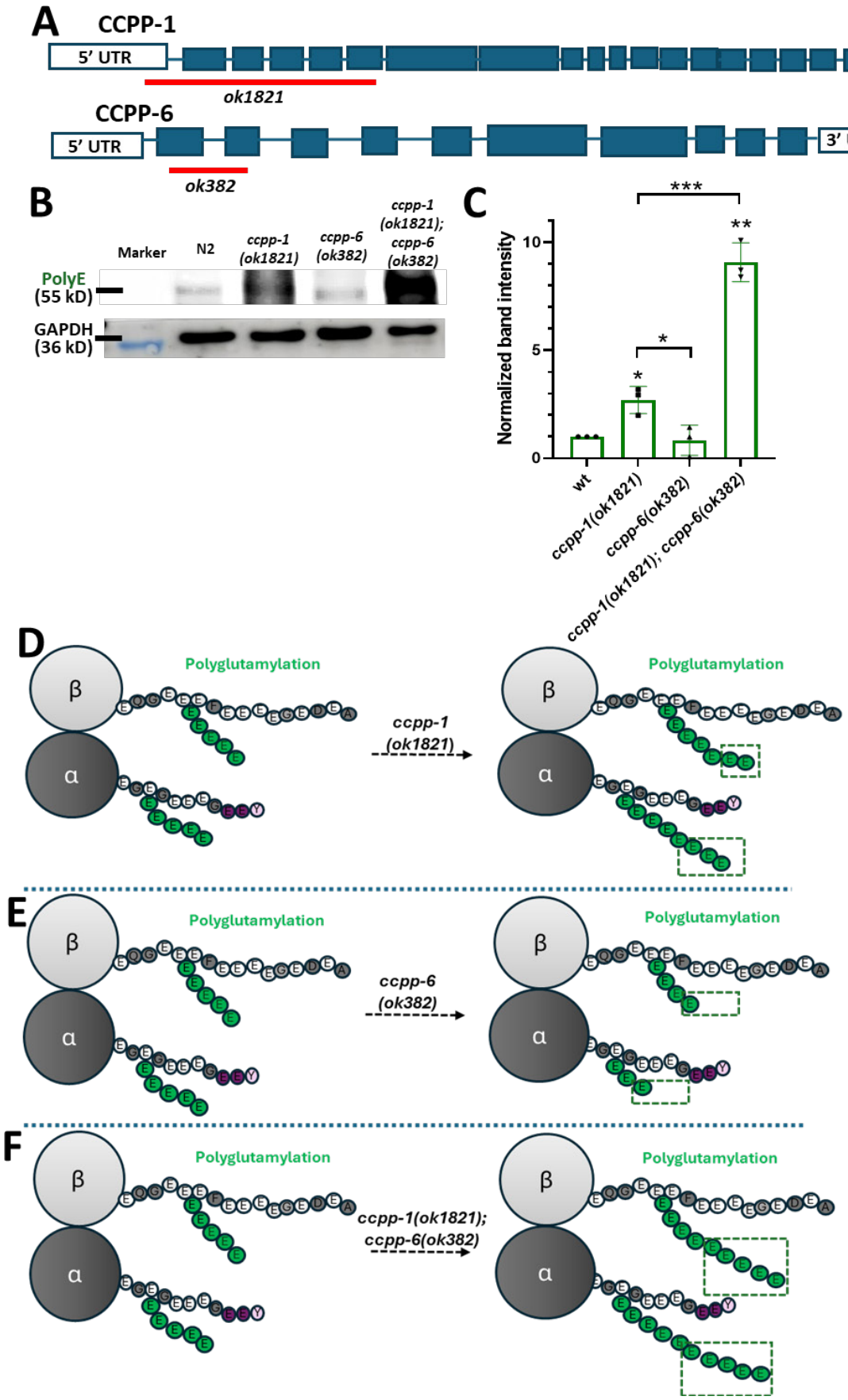

FIGURE 2

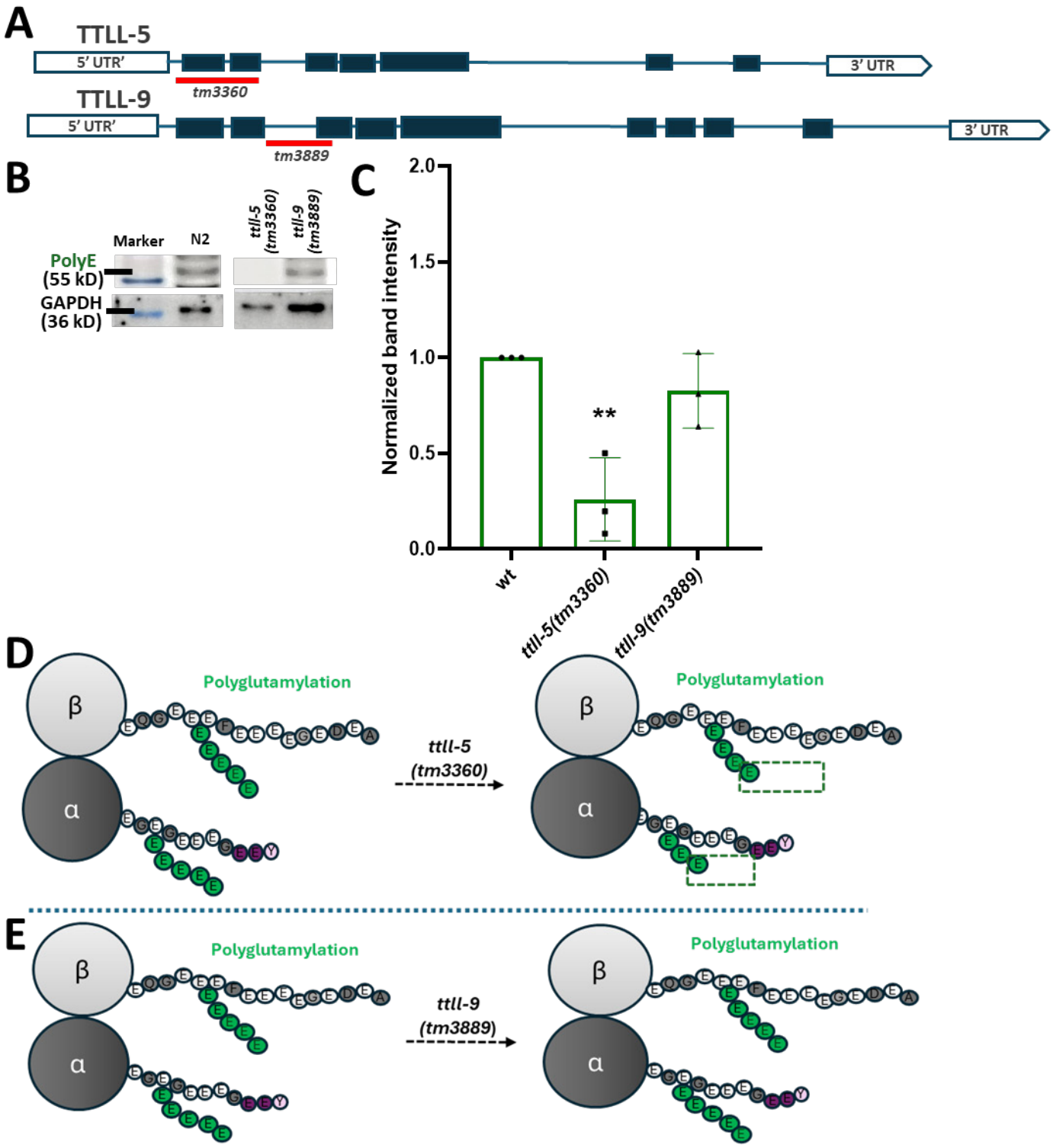
A
TTLL-5
5' UTR'
3' UTR
tm3360
TTLL-9
5' UTR'
3' UTR
tm3889
B
Marker
N2
ttll-5 (tm3360)
ttll-9 (tm3889)
PolyE (55 kD)
GAPDH (36 kD)
C
Normalized band intensity
2.0
1.5
1.0
0.5
0.0
**
wt
ttll-5(tm3360)
ttll-9(tm3889)
D
β
α
Polyglutamylation
ttll-5 (tm3360)
Polyglutamylation
E
β
α
Polyglutamylation
ttll-9 (tm3889)
Polyglutamylation

FIGURE 3

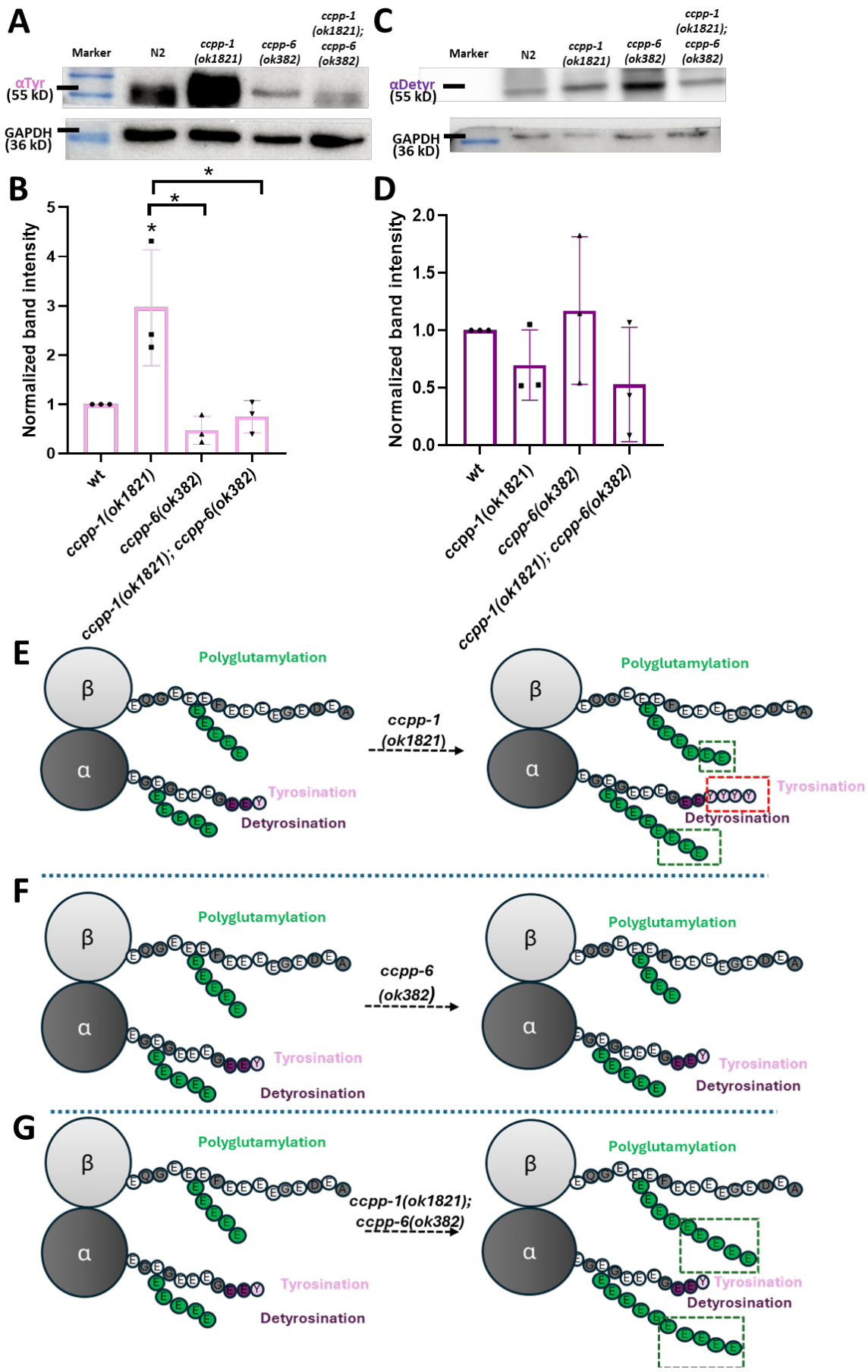
A
Marker
N2
ccpp-1 (ok1821)
ccpp-6 (ok382)
ccpp-1 (ok1821); ccpp-6 (ok382)
αTyr (55 kD)
GAPDH (36 kD)
C
αDetyr (55 kD)
B
Normalized band intensity
wt
ccpp-1(ok1821)
ccpp-6(ok382)
ccpp-1(ok1821); ccpp-6(ok382)
D
E
Polyglutamylation
Tyrosination
Detyrosination
ccpp-1 (ok1821)
F
ccpp-6 (ok382)
G
ccpp-1(ok1821); ccpp-6(ok382)

FIGURE 4

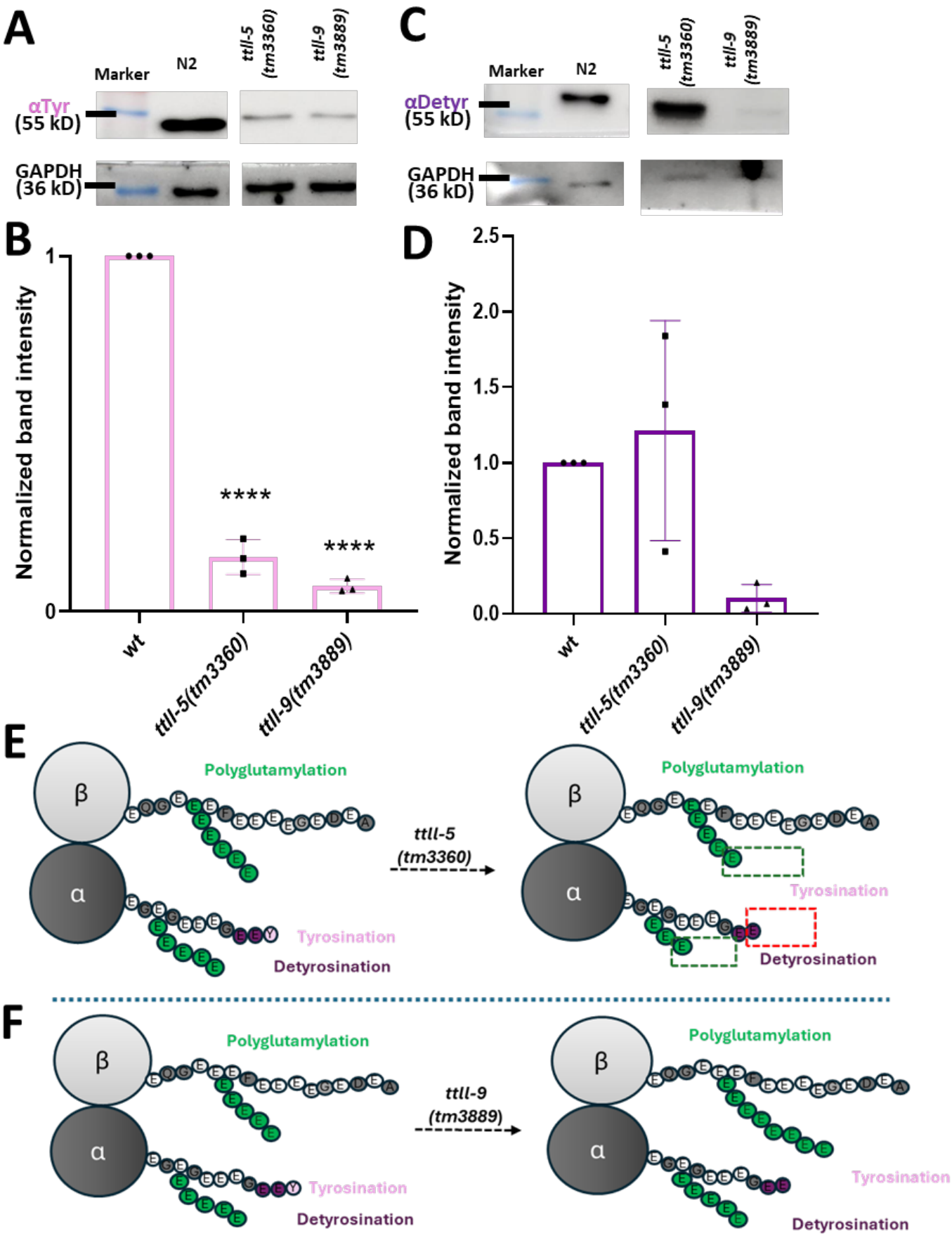
A
Marker
N2
ttl-5 (tm3360)
ttl-9 (tm3889)
αTyr (55 kD)
GAPDH (36 kD)
C
Marker
N2
ttl-5 (tm3360)
ttl-9 (tm3889)
αDetyr (55 kD)
GAPDH (36 kD)
B
Normalized band intensity
1
0
****
****
wt
ttl-5(tm3360)
ttl-9(tm3889)
D
Normalized band intensity
2.5
2.0
1.5
1.0
0.5
0.0
wt
ttl-5(tm3360)
ttl-9(tm3889)
E
β
α
Polyglutamylation
Tyrosination
Detyrosination
ttll-5 (tm3360)
Polyglutamylation
Tyrosination
Detyrosination
F
β
α
Polyglutamylation
Tyrosination
Detyrosination
ttll-9 (tm3889)
Polyglutamylation
Tyrosination
Detyrosination

FIGURE 5

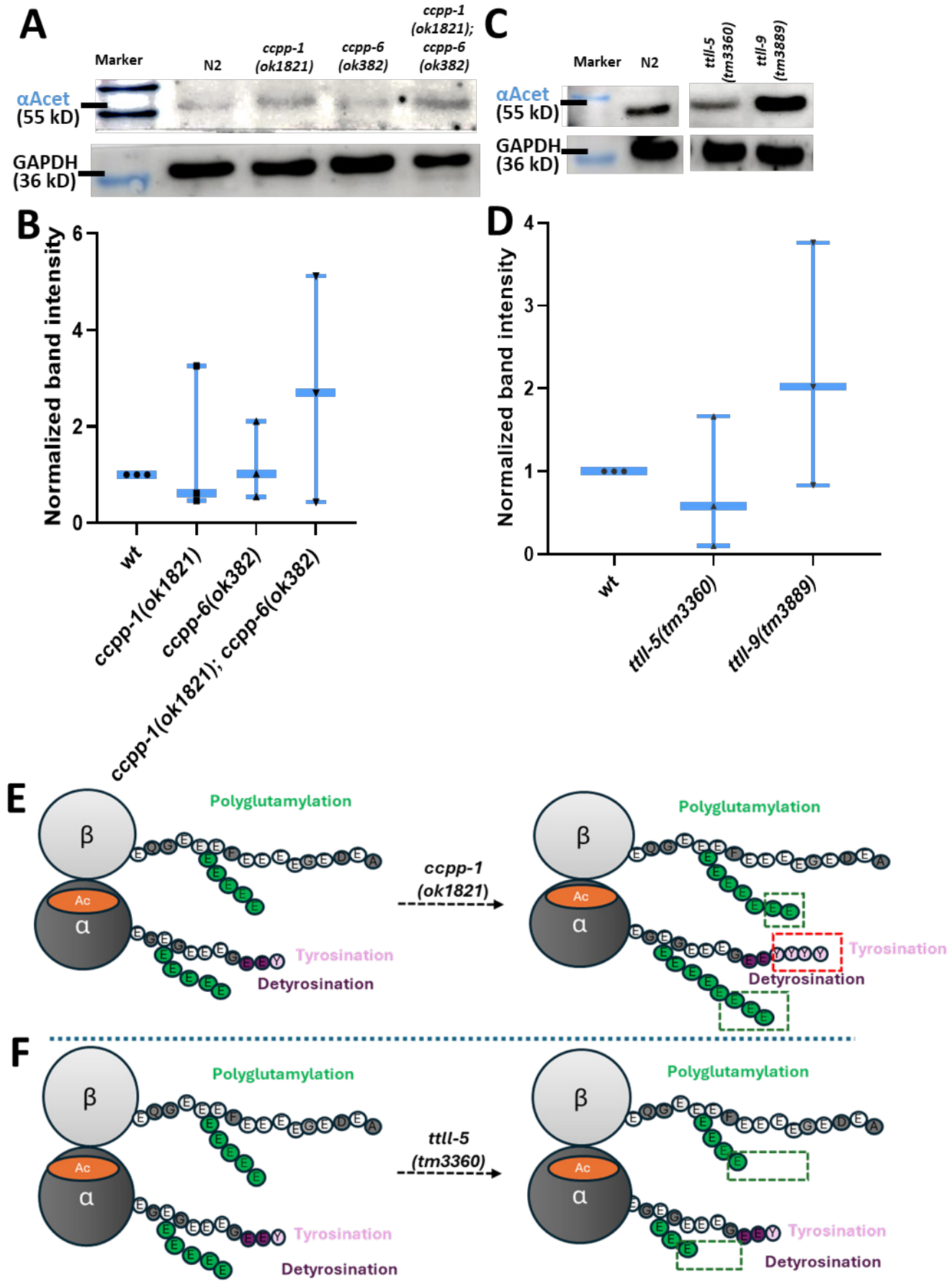
A
Marker
N2
ccpp-1 (ok1821)
ccpp-6 (ok382)
ccpp-1 (ok1821); ccpp-6 (ok382)
αAcet (55 kD)
GAPDH (36 kD)
C
Marker
N2
ttll-5 (tm3360)
ttll-9 (tm3889)
αAcet (55 kD)
GAPDH (36 kD)
B
Normalized band intensity
0
2
4
6
wt
ccpp-1(ok1821)
ccpp-6(ok382)
ccpp-1(ok1821); ccpp-6(ok382)
D
Normalized band intensity
0
1
2
3
4
wt
ttll-5(tm3360)
ttll-9(tm3889)
E
β
Ac
α
Polyglutamylation
Tyrosination
Detyrosination
ccpp-1 (ok1821)
F
ttll-5 (tm3360)

FIGURE 6

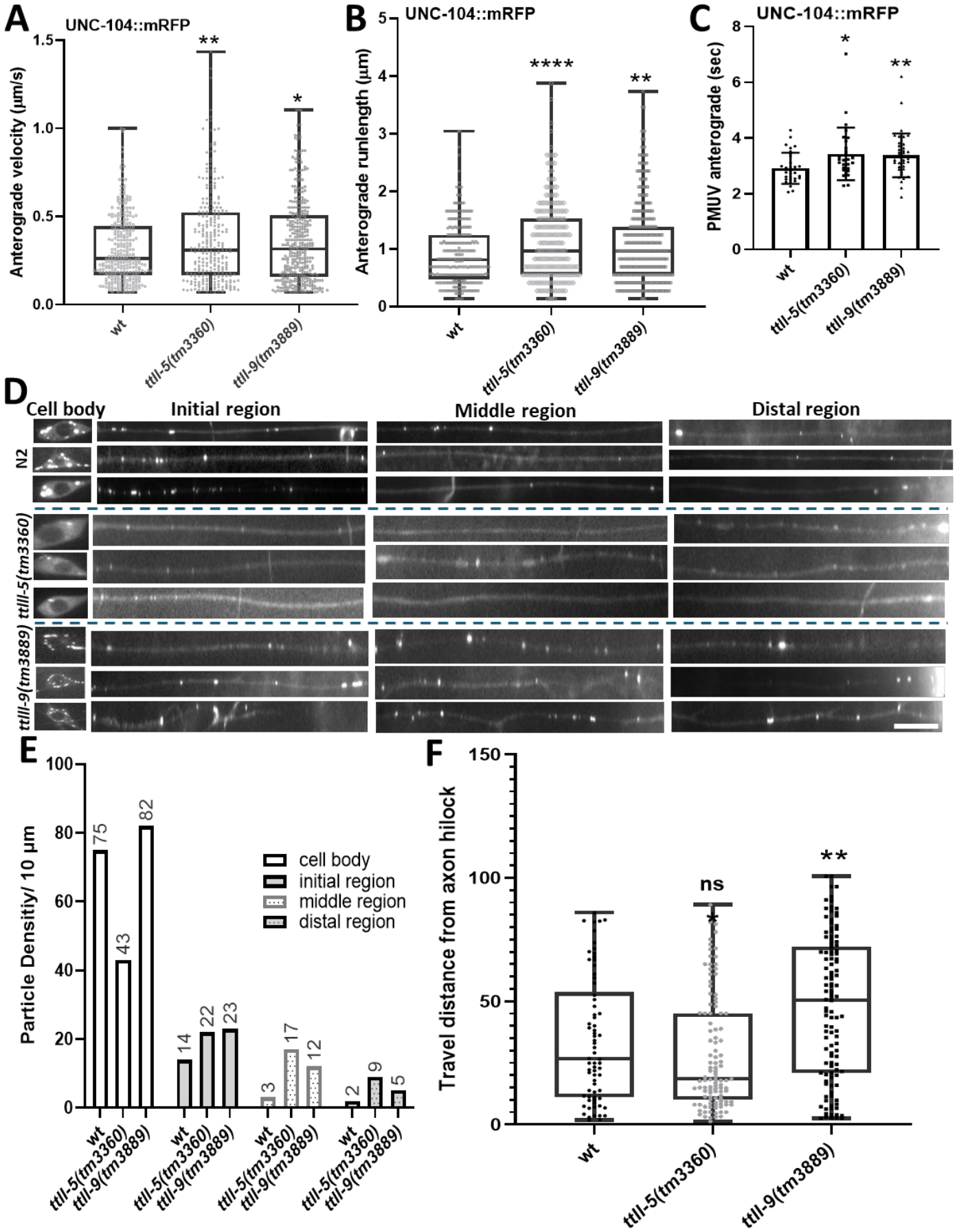
A
UNC-104::mRFP
Anterograde velocity (µm/s)
1.5
1.0
0.5
0.0
**
*
wt
ttll-5(tm3360)
ttll-9(tm3889)
B
UNC-104::mRFP
Anterograde runlength (µm)
5
4
3
2
1
0
****
**
wt
ttll-5(tm3360)
ttll-9(tm3889)
C
UNC-104::mRFP
PMUV anterograde (sec)
8
6
4
2
0
*
**
wt
ttll-5(tm3360)
ttll-9(tm3889)
D
Cell body
Initial region
Middle region
Distal region
N2
ttll-5(tm3360)
ttll-9(tm3889)
E
Particle Densitiy/ 10 µm
100
80
60
40
20
0
75
43
82
14
22
23
3
17
12
2
9
5
cell body
initial region
middle region
distal region
wt
ttll-5(tm3360)
ttll-9(tm3889)
F
Travel distance from axon hilock
150
100
50
0
ns
*
**
wt
ttll-5(tm3360)
ttll-9(tm3889)

FIGURE 7

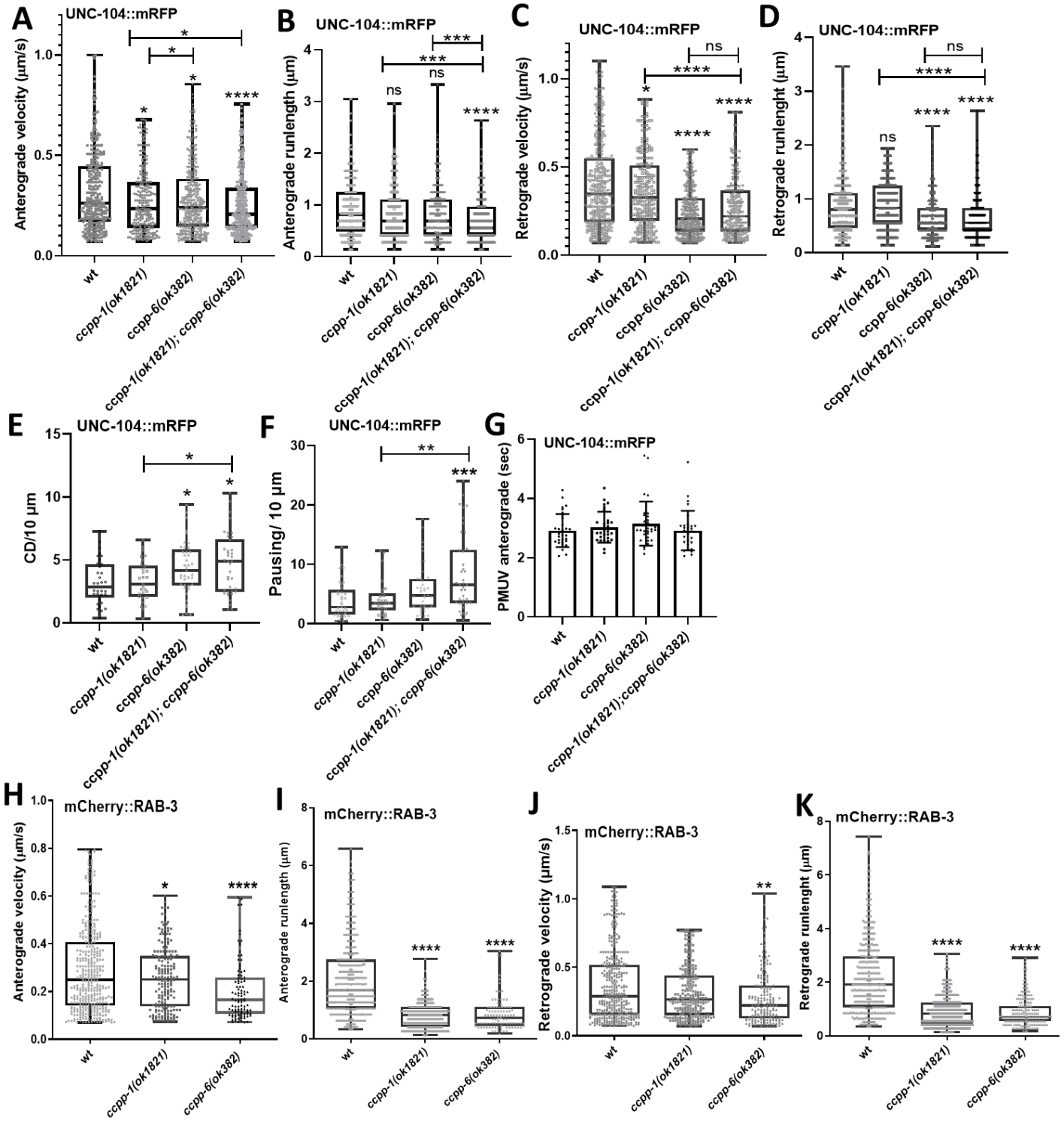
A
UNC-104::mRFP
Anterograde velocity (µm/s)
B
UNC-104::mRFP
Anterograde runlength (µm)
C
UNC-104::mRFP
Retrograde velocity (µm/s)
D
UNC-104::mRFP
Retrograde runlenght (µm)
E
UNC-104::mRFP
CD/10 µm
F
UNC-104::mRFP
Pausing/ 10 µm
G
UNC-104::mRFP
PMUV anterograde (sec)
H
mCherry::RAB-3
Anterograde velocity (µm/s)
I
mCherry::RAB-3
Anterograde runlength (µm)
J
mCherry::RAB-3
Retrograde velocity (µm/s)
K
mCherry::RAB-3
Retrograde runlenght (µm)
wt
ccpp-1(ok1821)
ccpp-6(ok382)
ccpp-1(ok1821); ccpp-6(ok382)
ns

FIGURE 8

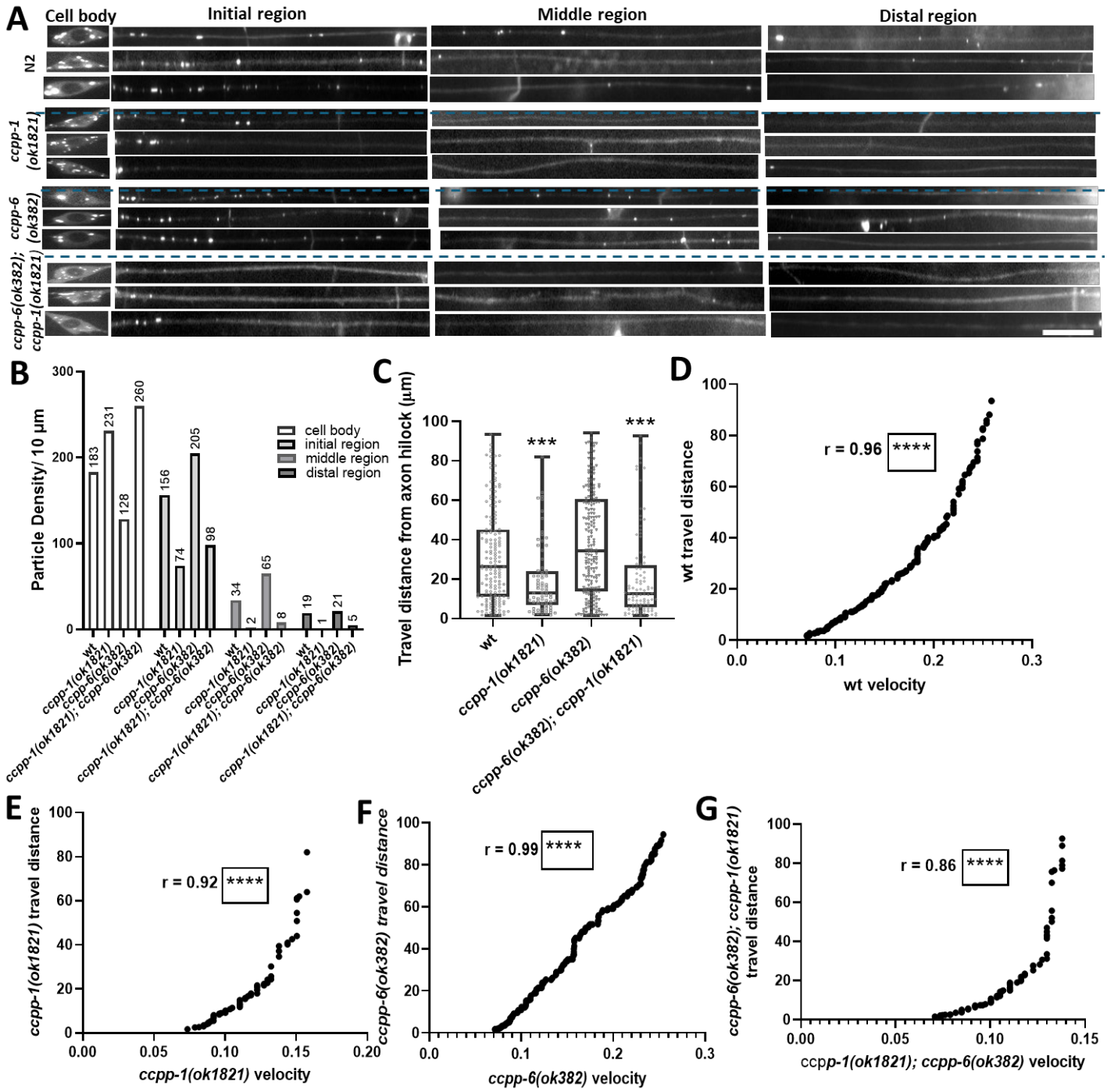
A
Cell body
Initial region
Middle region
Distal region
N2
ccpp-1 (ok1821)
ccpp-6 (ok382)
ccpp-6(ok382); ccpp-1(ok1821)
B
Particle Density/ 10 µm
cell body
initial region
middle region
distal region
183
231
128
260
156
74
205
98
34
2
65
8
19
1
21
5
wt
ccpp-1(ok1821)
ccpp-6(ok382)
ccpp-1(ok1821); ccpp-6(ok382)
C
Travel distance from axon hillock (µm)
***
***
wt
ccpp-1(ok1821)
ccpp-6(ok382)
ccpp-6(ok382); ccpp-1(ok1821)
D
wt travel distance
r = 0.96
****
wt velocity
E
ccpp-1(ok1821) travel distance
r = 0.92
****
ccpp-1(ok1821) velocity
F
ccpp-6(ok382) travel distance
r = 0.99
****
ccpp-6(ok382) velocity
G
ccpp-6(ok382); ccpp-1(ok1821) travel distance
r = 0.86
****
ccpp-1(ok1821); ccpp-6(ok382) velocity

FIGURE 9

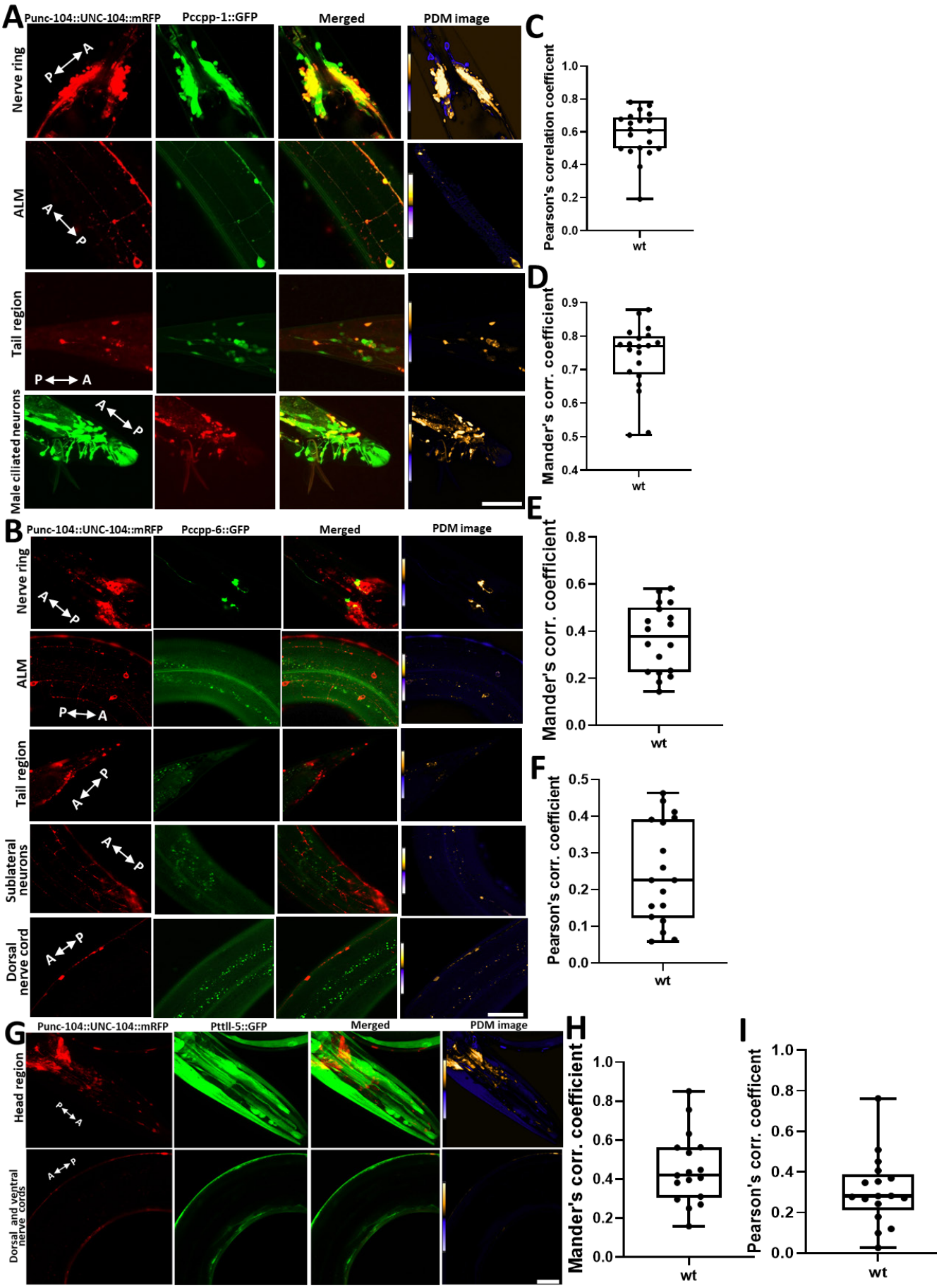
A
Punc-104::UNC-104::mRFP
Pccpp-1::GFP
Merged
PDM image
Nerve ring
ALM
Tail region
Male ciliated neurons
B
Punc-104::UNC-104::mRFP
Pccpp-6::GFP
Merged
PDM image
Nerve ring
ALM
Tail region
Sublateral neurons
Dorsal nerve cord
C
Pearson's correlation coefficent
wt
D
Mander's corr. coefficient
wt
E
Mander's corr. coefficient
wt
F
Pearson's corr. coefficient
wt
G
Punc-104::UNC-104::mRFP
Pttll-5::GFP
Merged
PDM image
Head region
Dorsal and ventral nerve cords
H
Mander's corr. coefficient
wt
I
Pearson's corr. coefficent
wt

FIGURE 10

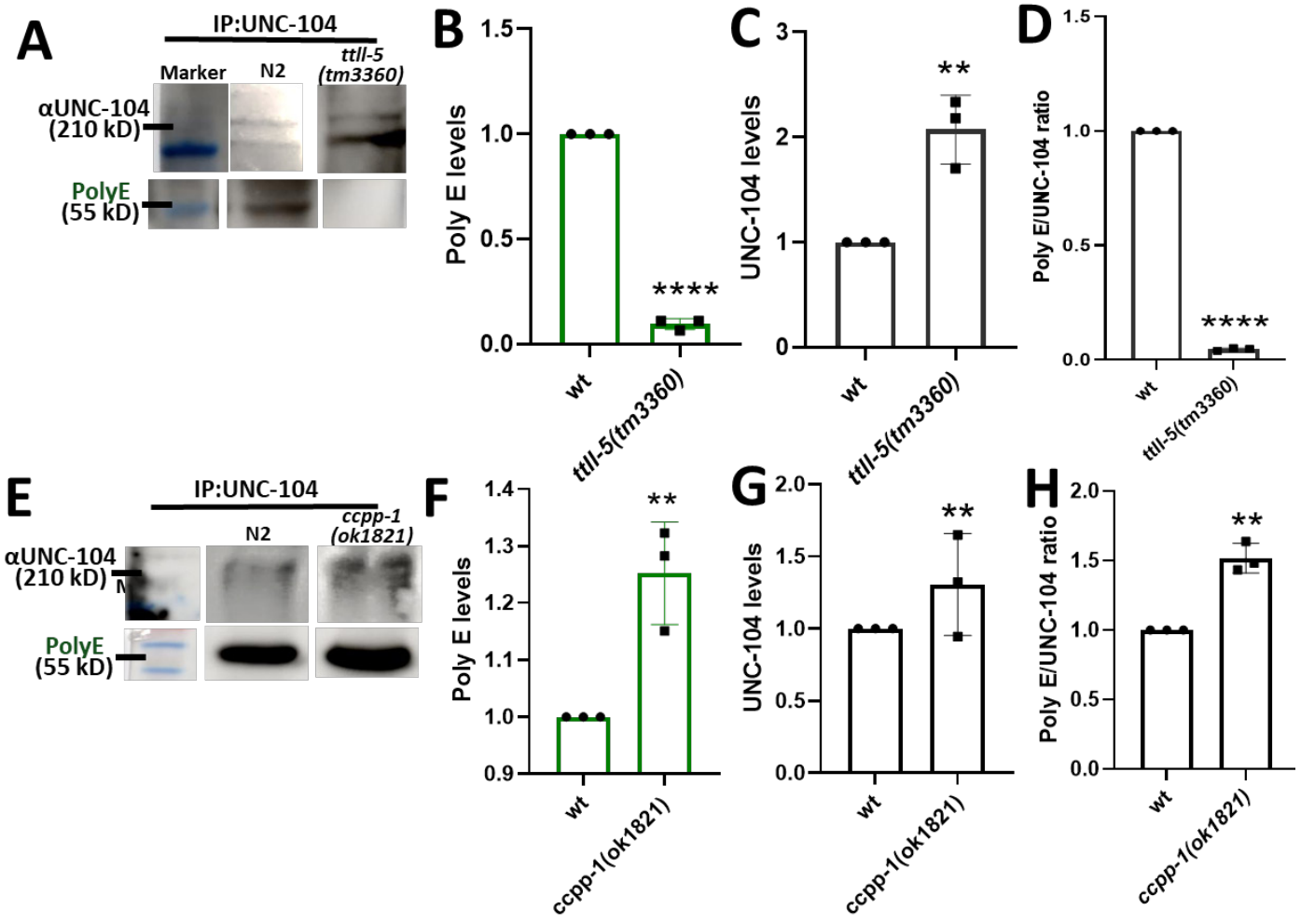
A
IP:UNC-104
Marker
N2
ttll-5 (tm3360)
αUNC-104 (210 kD)
PolyE (55 kD)
B
Poly E levels
1.5
1.0
0.5
0.0
****
wt
ttll-5(tm3360)
C
UNC-104 levels
3
2
1
0
**
wt
ttll-5(tm3360)
D
Poly E/UNC-104 ratio
1.5
1.0
0.5
0.0
****
wt
ttll-5(tm3360)
E
IP:UNC-104
N2
ccpp-1 (ok1821)
αUNC-104 (210 kD)
PolyE (55 kD)
F
Poly E levels
1.4
1.3
1.2
1.1
1.0
0.9
**
wt
ccpp-1(ok1821)
G
UNC-104 levels
2.0
1.5
1.0
0.5
0.0
**
wt
ccpp-1(ok1821)
H
Poly E/UNC-104 ratio
2.0
1.5
1.0
0.5
0.0
**
wt
ccpp-1(ok1821)

FIGURE 11

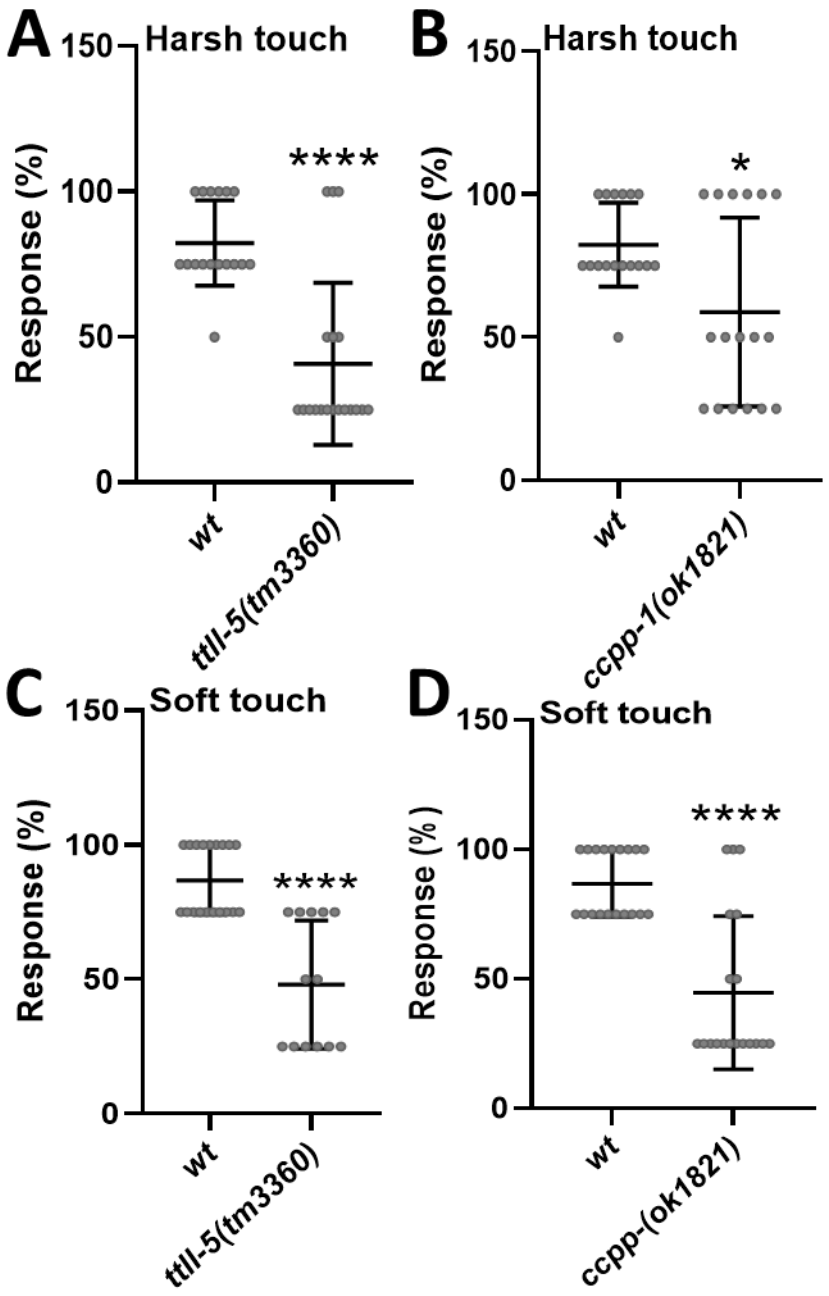
A
Harsh touch
Response (%)
150
100
50
0
****
wt
ttll-5(tm3360)
B
Harsh touch
Response (%)
150
100
50
0
*
wt
ccpp-1(ok1821)
C
Soft touch
Response (%)
150
100
50
0
****
wt
ttll-5(tm3360)
D
Soft touch
Response (%)
150
100
50
0
****
wt
ccpp-(ok1821)

FIGURE 12

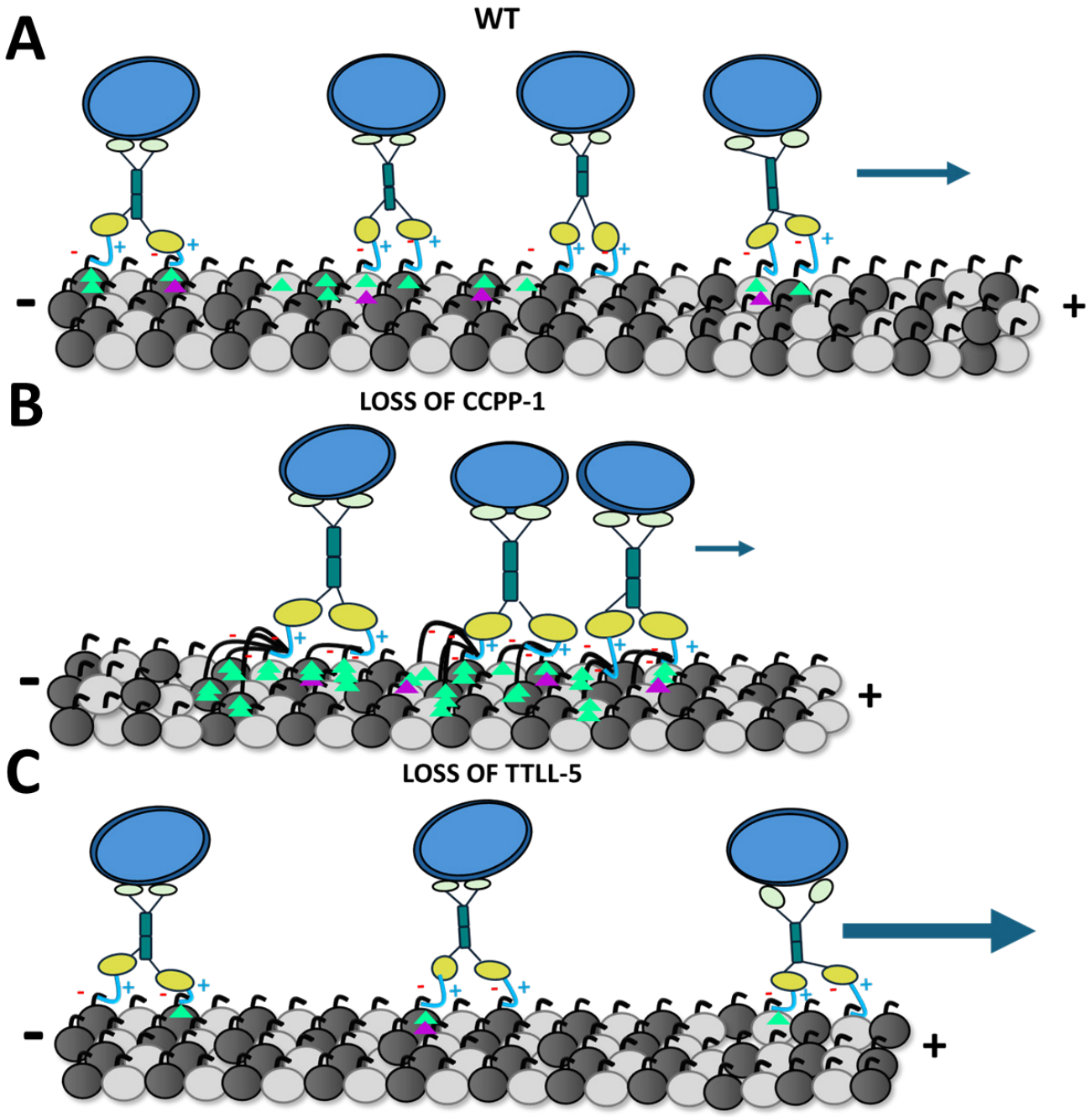

FIGURE LEGENDS

Figure. 1: CCPP-1, but not CCPP-6, cleaves polyglutamylated tubulin. (A) Wild type gene structures of *ccpp-1* and *ccpp-6* as well as available alleles. Red lines indicate deletions in the respective alleles. (B) Western blot employing an antibody detecting polyglutamylated tubulin (PolyE) in *ccpp-1* and *ccpp-6* single mutants as well as in *ccpp-1;ccpp-6* double mutants. (C) Quantification of data shown in (B). (D-F) Schematic representations of tubulin polyglutamylation effects revealed in *ccpp-1* (D), *ccpp-6* (E), and *ccpp-1;ccpp-6* mutants (F). Dark green boxes highlight changes in polyglutamylation chains. For panel C, one-way ANOVA with Dunnett's test was used for multiple comparisons (*p<0.05, **p<0.005). For two-group comparisons, an unpaired, two-tailed Student's t-test was performed (*p<0.05***p< 0.001). Box and whisker plots represent the maximum value, upper quartile, median, lower quartile, and minimum value. Experiments carried out in triplicates.

Figure. 2: Polyglutamylated tubulin levels in *ttll* mutants. (A) Gene structures of *ttll-5 and ttll-9* with deletions in mutant alleles highlighted in red. (B) Western blots revealing levels of polyE polyglutamylated tubulin in N2, *ttll-5* and *ttll-9* mutants. (C) Quantification of Western blot data shown in (B). (D+E) Schematic representations of revealed results for polyglutamylated tubulin in *ttll-5* (D) and *ttll-9* (E). For panel C, one-way ANOVA with Dunnett's test was used for multiple comparisons with **p<0.005. Box and whisker plots represent the maximum value, upper quartile, median, lower quartile, and minimum value. Experiments replicated in triplicates. Dark green boxes indicate polyglutamylated tubulin modifications.

Figure. 3: Changes in tyro- and detyrosination of tubulin in *ccpp* single and double mutants: (A+C) Western blots showing signals of (A) anti-tyrosinated tubulin and (C) anti-detyrosinated tubulin in deglutamylase single and double mutants. (B+D) Quantification of data from (A) and (C). (E+G) Schematic representations of changes in tyro/detyrosinated tubulin in *ccpp-1* (E), *ccpp-6* (F), and *ccpp-1;ccpp-6* mutants (G). For panels B+D, one-way ANOVA with Dunnett's test was used for multiple comparisons (*p<0.05). For two-group comparisons, an unpaired, two-tailed Student's t-test was performed (*p<0.05). Box and whisker plots represent the maximum value, upper quartile, median, lower quartile, and minimum

value. Each experiment was performed in triplicates. Dark green boxes highlight changes in polyglutamylated tubulin modifications. Red box highlights change in tyro/detyrosinated tubulin modifications.

Figure. 4: Effect of tyro- and detyrosination in *ttll-5* and *ttll-9* mutants: (A+C) Western blots showing signals of (A) anti-tyrosinated tubulin and (C) anti-detyrosinated tubulin in *ttll-5(tm3360)* and *ttll-9(tm3889)* mutants. (B+D) Quantification of data from (A) and (C). (E+G) Schematic representations of changes in tyro/detyrosinated tubulin in *ttll-5* (E) and *ttll-9* (F) mutants. For panels B+D, one-way ANOVA with Dunnett's test was used for multiple comparisons with ****$p<0.0001$. Box and whisker plots represent the maximum value, upper quartile, median, lower quartile, and minimum value. Each experiment was performed in triplicate. Dark green boxes highlight changes in polyglutamylated tubulin modifications. Red box highlights change in tyro/detyrosinated tubulin modifications.

Figure. 5: Effects of acetylated tubulin in deglutamylase and polyglutamylase mutants: (A+C) Western blots showing signals of α-acetylated tubulin levels in deglutamyalse mutants (A) and polyglutamylase mutants (C). (B+D) Quantification of data from (A) and (C). (E+F) Schematic representations of changes in acetylated tubulin in *ccpp-1(ok1821)* and *ttll-5(tm3360)* mutants. For panels B+D, one-way ANOVA with Dunnett's test was used for multiple comparisons. Box and whisker plots represent the maximum value, upper quartile, median, lower quartile, and minimum value. Each experiment was performed in triplicate. Dark green boxes indicate polyglutamylated tubulin modifications. Red boxes indicate modification of tyro/detyrosinated tubulin. Orange circles highlight acetylated tubulin.

Figure 6: Effect of hypoglutamylated tubulin on UNC-104 motility. (A) Anterograde velocity of UNC-104::mRFP in wild type, *ttll-5* and *ttll-9* mutants. (B) UNC-104 anterograde event run lengths. (C) UNC-104's persistent movement in anterograde direction in wild type, *ttll-5* and *ttll-9* mutants. (D) Stacks of ALM neurons in wild type and *ttll-5(tm3360)* and *ttll-9(tm3889)* mutants. (E) Density of UNC-104 particles per 10 µm in cell body, initial, middle and distal regions . (F) Travel distances of UNC-104 (data taken from Fig. 6D). Analyzed total events: wt = 1009, *ttll-5*(*tm3360*) = 710 and *ttll-9*(*tm3889*) = 1143. One-way ANOVA with Dunnett's test with *$p<0.05$ and **$p<0.005$ in (A). n = 11 worms for wt, *ttll-5(tm3360)* and

ttll-9(tm3889) mutants in (D). Non-parametric Kruskal-Wallis one-way ANOVA with Dunn's test for multiple comparisons with *p<0.05, **p<0.005 and ****p<0.0001 in (B+C, F). Box and whisker graphs represent maximum value, upper quartile, median, lower quartile and minimum value. Scale bar: 10 µm.

Figure 7: Hyperglutamylated tubulin negatively affects kinesin-3-based axonal transport. (A) Anterograde velocity of UNC-104::mRFP in single *ccpp-1*, *ccpp-6* and *ccpp-1;ccpp-6* double mutants. (B) UNC-104 anterograde event run lengths. (C) UNC-104 retrograde velocity and (D) event run lengths. (E) Directional changes of UNC-104 within 10 µm. (F) UNC-104's pauses per 10 µm. (G) UNC-104's persistent movement in anterograde direction. (H) RAB-3 anterograde velocity. (I) RAB-3 anterograde run length. (K) RAB-3 retrograde velocity. (L) RAB-3 retrograde run length, analyzed total events for A-G: wt = 1009, *ccpp-1*(*ok1821*) = 781, *ccpp-6*(*ok382*) = 1108, *ccpp-1*(*ok1821*)*;ccpp-6*(*ok382*) = 1028. Analyzed total events for H-K: wt = 798, *ccpp-1(ok1821)* = 652 and *ccpp-6(ok382)* = 412. One-way ANOVA with Dunnett's test with *p<0.05, **p<0.005 and **** p<0.0001 in (A+C+H+J). Non-parametric Kruskal-Wallis one-way ANOVA with Dunn's test for multiple comparisons with *p<0.05, **p<0.005, ***p< 0.001, and ****p<0.0001 in (B, D-G, I+K). For two group comparisons in (A) unpaired Student's t-test with *p<0.05 was used. For (B, D-F) we use unpaired, non-parametric Mann-Whitney test with *p<0.05, **p<0.01, ***p<0.001. Box and whisker graphs represent maximum value, upper quartile, median, lower quartile and minimum value.

Figure 8: Effect of deglutamylase enzymes on UNC-104 axonal cluster patterns. (A) Stacks of ALM neurons (after digital straightening) to examine UNC-104 cluster patterns in single and double deglutamylase mutants. (B) Density of UNC-104 particles per 10 µm in cell body, initial, middle and distal regions . (C) Travel distances of UNC-104 (data taken from Fig. 7A). (D-G) Correlation between UNC-104 motility (taken from Fig. 7A) and UNC-104 particle travel distance in ALM neurons (taken from Fig. 8C) in (D) wild type, (E) *ccpp-1*(*ok1821*) mutants, (F) *ccpp-6*(*ok382*) mutants and (G) *ccpp-1*(*ok1821*)*;ccpp-6*(*ok382*) double mutants. N = 20-25 worms per experimental group for cluster analysis in (A-C). Non-parametric Kruskal-Wallis one-way ANOVA with Dunn's test for multiple comparisons with ***p< 0.001 in (C). R values based on Pearson's correlation coefficient and p values determined using Student's t-test for two

group comparisons with ****p<0.0001. Box and whisker graphs represent maximum value, upper quartile, median, lower quartile and minimum value. Scale bar: 10 µm.

Figure 9: Colocalization between UNC-104 and promoter fusions of deglutamylase and polyglutamylase enzymes. (A+B) Colocalization between UNC-104 and (A) ccpp-1 promoter fusion and (B) ccpp-6 promoter fusion in head and body neurons. (C+F) Mander's and Pearson's coefficients from data shown in (A+B). (G) Colocalization between UNC-104 and ttll-5 promoter fusion in head sensory neurons, epidermis and dorsal and ventral nerve cords. (H+I) Mander's and Pearson's coefficients from data represented in (G). Box and whisker graphs represent maximum value, upper quartile, median, lower quartile and minimum value. N = 18-20 worms. A = anterior, P = posterior directions. Scale bar: 10 µm.

Figure 10: Polyglutamylated tubulin directly interacts with UNC-104. (A+E) Co-immunoprecipitation assays showing the interaction between UNC-104 and polyglutamylated tubulin using lysates from whole worms expressing UNC-104::mRFP in (A) wt and polyglutamylase *ttll-5*(*tm3360*) mutants and (E) wt and deglutamylase *ccpp-1*(*ok1821*) mutants. (B-D) Co-IP quantification of (B) polyglutamylated tubulin, (C) UNC-104 protein and (D) PolyE/UNC-104 ratio in wt and *ttll-5*(*tm3360*) mutants. (F-H) Co-IP quantification of (F) polyglutamylated tubulin, (G) UNC-104 protein and (H) PolyE/UNC-104 ratio in wt and *ccpp-1*(*ok1821*) mutants. For two-group comparisons, unpaired, two-tailed Student's t-test was employed with **p<0.005 and ***p< 0.001. Number of trials for each experimental group: 3

Figure. 11: Harsh and soft touch assays in hypo- and hyperglutamylated tubulin mutants. (A+B) Harsh touch assays in (A) *ttll-5(tm3360)* mutants and (B) *ccpp-1(ok1821)* mutants. (C+D) Soft touch assays in (C) *ttll-5(tm3360)* mutants and (D) *ccpp-1(ok1821)* mutants. For two-group comparisons, unpaired, non-parametric Mann-Whitney test with *p<0.05 and ****p<0.0001. n = 13-19 worms.

Figure. 12: Model summarizing the findings of this study. (A) UNC-104 motors moving on a microtubule in wild type animals, (B) *ttll-5* mutant and (C) *ccpp-1* mutant. The positively charged K-loop of kinesin-3 (light blue hook) interacts with the negatively charged C-terminal tail (E-hook, black hook) of tubulin. Green triangles represent polyglutamylation, while magenta triangles indicate tyrosination. Arrows show

average velocity, reduced velocity and increased velocity. Increased polyglutamylation leads to increased negative surface charges of the microtubule increasingly trapping and immobilizing UNC-104. (B) in addition, increased tyrosination leads to less stable microtubules.

SUPPLEMENTARY FIGURES

SUPPPL. FIG. S1

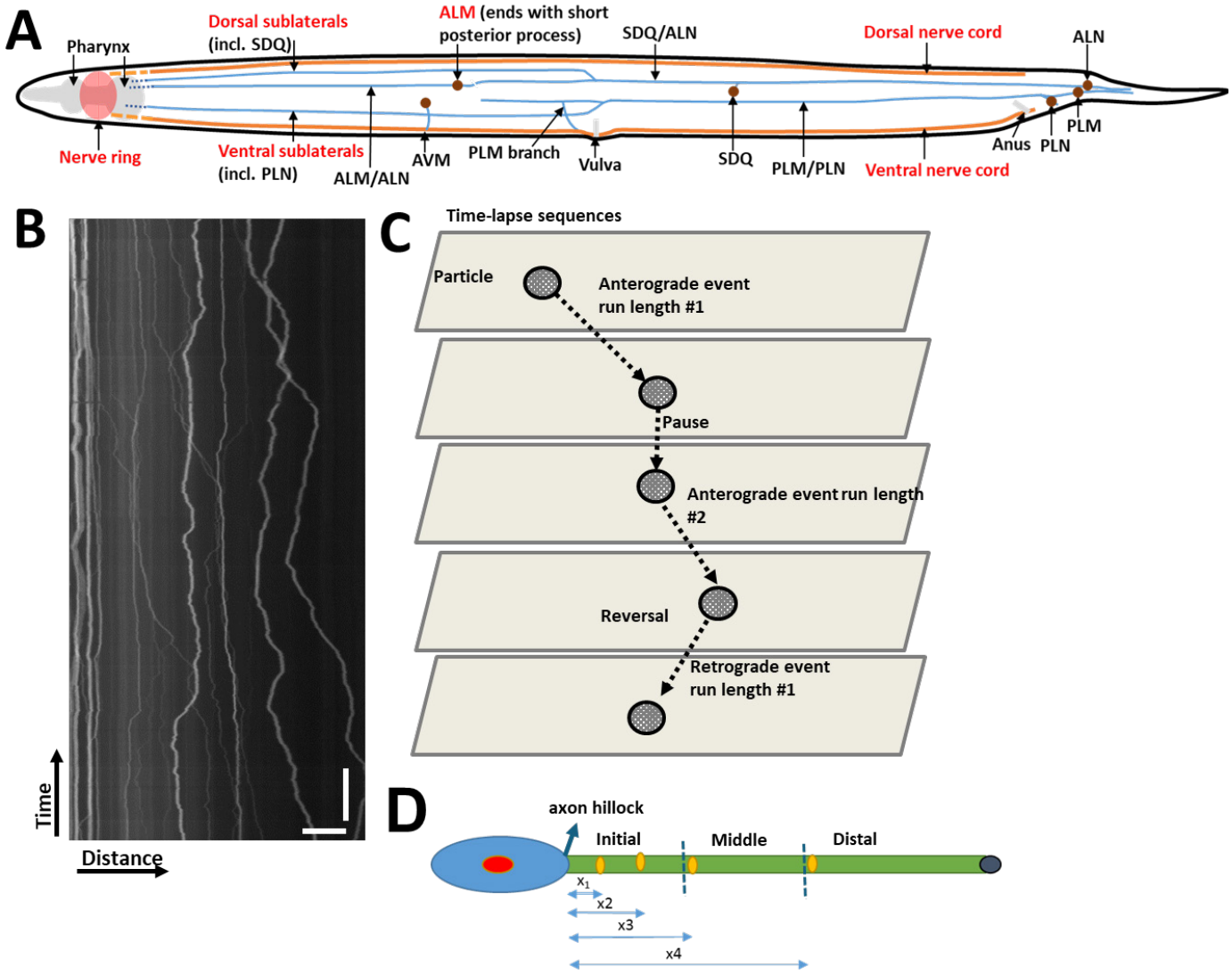

SUPPPL. FIG. S2

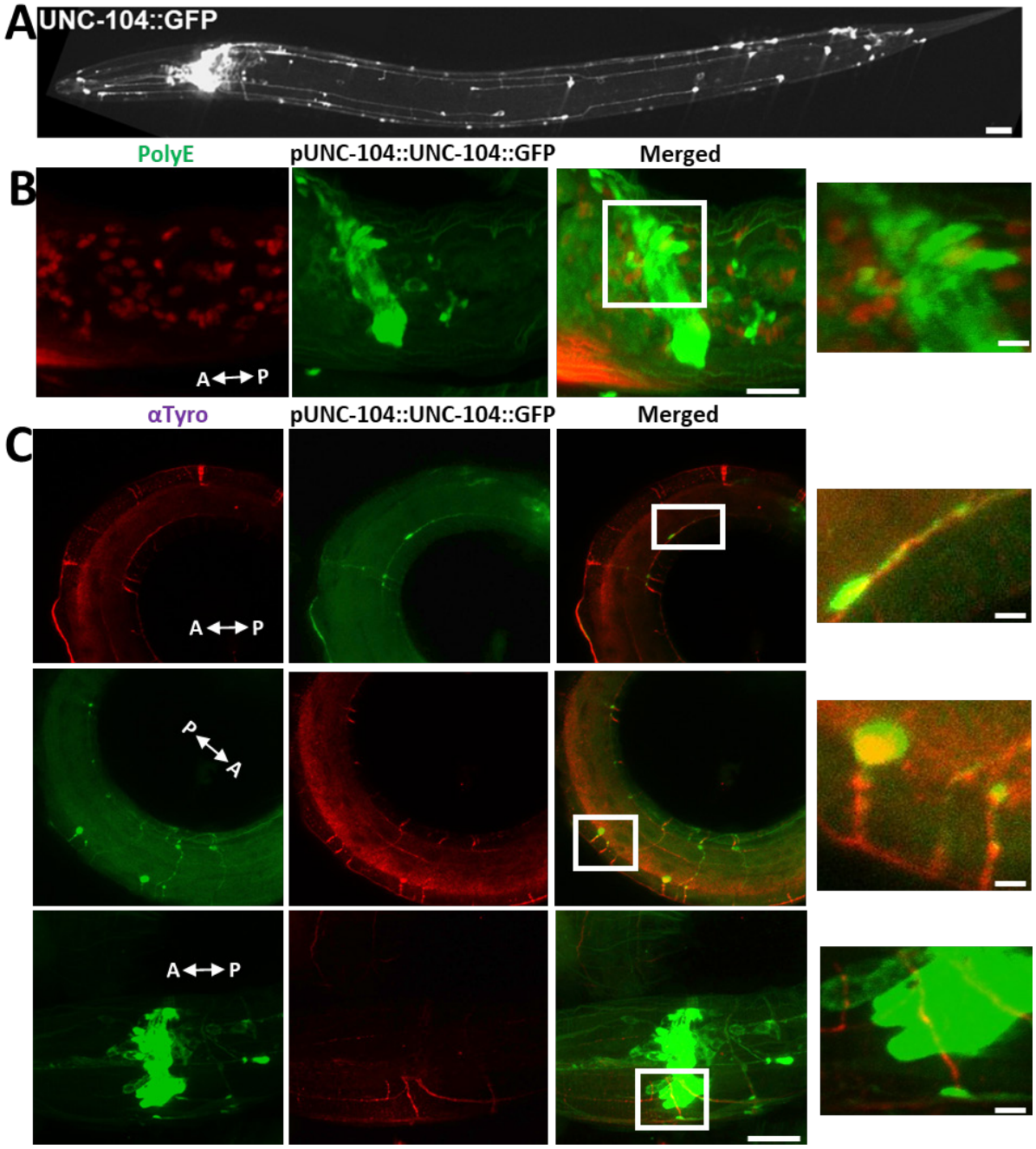

SUPPPL. FIG. S3

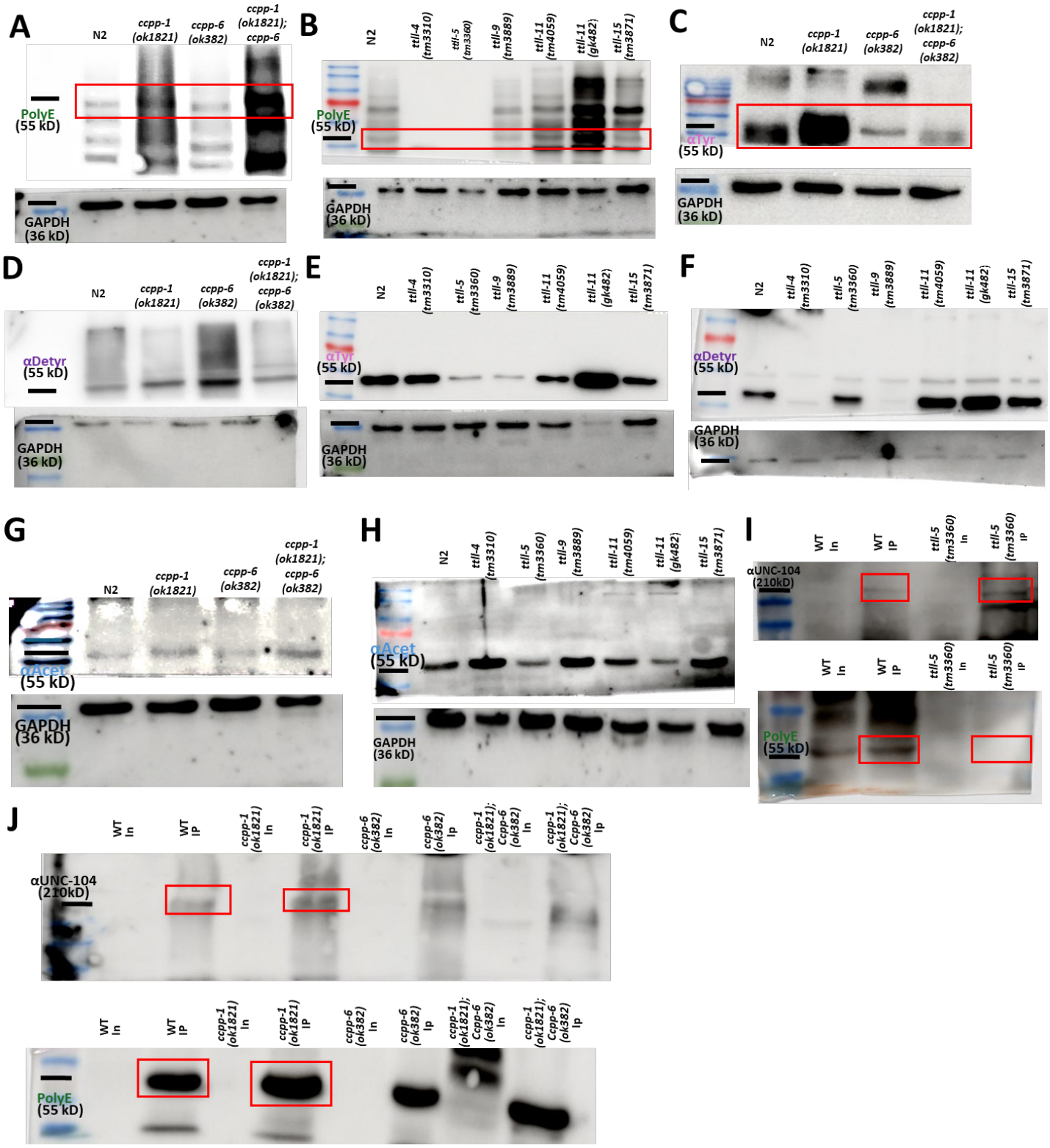

SUPPLEMENTARY FIGURE LEGENDS

Suppl. Figure S1: Diagrammatic schemes of mentioned neurons, kymograph analysis as well as cluster analysis methods. (A) Simplified scheme of the nervous system in *C. elegans* (cell bodies in brown color and axons in light blue color). (B) Example of a kymograph and (C) a diagrammatic scheme of various motility parameters generated from a kymograph. (D) Schematic diagram of a neuron with blue, double-sided arrows indicating the distances traveled from the axon hillock to farther distal regions. One-sided arrow indicates the axon hillock from the cell body and dotted lines separate the initial, middle and distal regions . Scale bars: vertical = 30 s, horizontal = 10 µm.

Suppl. Figure S2: Whole worm immunostaining to determine the localization of polyglutamylated and tyrosinated tubulin in *C. elegans*. (A) Expression of UNC-104::GFP in wild type worms serving as a pan-neuronal marker. (B) Staining of long (PolyE) polyglutamylated tubulin in UNC-104::GFP expressing worms. (C) αTyrosinated tubulin stained in worms expressing UNC-104::GFP. A = Anterior, P = Posterior, white boxes highlighting selected regions for the insets. Scale bars: 10 µm; inset: 50 nm

Suppl. Figure S3: Suppl. Figure S4: Representative raw images of Western blots and CO-IP (unmodified and boxed). (A) Upper panel: PolyE (55 kD) and lower panel: anti-GAPDH (36 kD) in N2 and deglutamylase mutants (from Fig. 1B). (B) Upper panel: PolyE (55 kD) and Lower panel: anti-GAPDH (36 kD) in N2 and polyglutamylase mutants (from Fig. 2B). (C) Upper panel: αTyrosinated tubulin (55 kD) and Lower panel: anti-GAPDH (36 kD) in N2 and deglutamylase mutants (from Fig. 3A). (D) Upper gel αDetyrosinated tubulin (55 kD) and lower panel αnti-GAPDH (36 kD) in N2 and deglutamylase mutants (from Fig. 3C). (E) Upper gel αTyrosinated tubulin (55 kD) and lower gel αnti-GAPDH (36 kD) in N2 and polgyglutamylase mutants (from Fig. 4A). (F) Upper gel αDetyrosinated tubulin (55 kD) and lower gel αnti-GAPDH (36 kD) in N2 and polgyglutamylase mutants (from Fig. 4C). (G) Upper gel αAcetylated tubulin (55 kD) and lower gel αnti-GAPDH (36 kD) in N2 and deglutamylase mutants (from Fig. 5A). (H) Upper gel αAcetylated tubulin (55 kD) and lower gel αnti-GAPDH (36 kD) in N2 and polyglutamylase mutants (from Fig. 5C). (I) Upper gel αUNC-104 (210 kD) and lower gel PolyE (55 kD) in wild type and

ttll-5(tm3360) mutants (from Fig. 10A). (J) Upper gel αUNC-104 (210 kD) and lower gel PolyE (55 kD) in wild type and deglutamylase mutants (from Fig. 10E).

REFERENCES

Ahmad FJ, Pienkowski TP, Baas PW (1993) Regional differences in microtubule dynamics in the axon. *J Neurosci* 13: 856-866

Aillaud C, Bosc C, Peris L, Bosson A, Heemeryck P, Van Dijk J, Le Friec J, Boulan B, Vossier F, Sanman LE *et al* (2017) Vasohibins/SVBP are tubulin carboxypeptidases (TCPs) that regulate neuron differentiation. *Science* 358: 1448-1453

Bayansan O, Bhan P, Chang CY, Barmaver SN, Shen CP, Wagner OI (2025) UNC-10/SYD-2 links kinesin-3 to RAB-3-containing vesicles in the absence of the motor's PH domain. *Neurobiol Dis* 204: 106766

Benoit M, Rao L, Asenjo AB, Gennerich A, Sosa H (2024) Cryo-EM unveils kinesin KIF1A's processivity mechanism and the impact of its pathogenic variant P305L. *Nat Commun* 15: 5530

Berezniuk I, Lyons PJ, Sironi JJ, Xiao H, Setou M, Angeletti RH, Ikegami K, Fricker LD (2013) Cytosolic carboxypeptidase 5 removes alpha- and gamma-linked glutamates from tubulin. *J Biol Chem* 288: 30445-30453

Berezniuk I, Vu HT, Lyons PJ, Sironi JJ, Xiao H, Burd B, Setou M, Angeletti RH, Ikegami K, Fricker LD (2012) Cytosolic carboxypeptidase 1 is involved in processing alpha- and beta-tubulin. *J Biol Chem* 287: 6503-6517

Bodakuntla S, Yuan X, Genova M, Gadadhar S, Leboucher S, Birling MC, Klein D, Martini R, Janke C, Magiera MM (2021) Distinct roles of alpha- and beta-tubulin polyglutamylation in controlling axonal transport and in neurodegeneration. *EMBO J* 40: e108498

Bonnet C, Boucher D, Lazereg S, Pedrotti B, Islam K, Denoulet P, Larcher JC (2001) Differential binding regulation of microtubule-associated proteins MAP1A, MAP1B, and MAP2 by tubulin polyglutamylation. *J Biol Chem* 276: 12839-12848

Borys F, Joachimiak E, Krawczyk H, Fabczak H (2020) Intrinsic and Extrinsic Factors Affecting Microtubule Dynamics in Normal and Cancer Cells. *Molecules* 25

Boucher D, Larcher JC, Gros F, Denoulet P (1994) Polyglutamylation of tubulin as a progressive regulator of in vitro interactions between the microtubule-associated protein Tau and tubulin. *Biochemistry* 33: 12471-12477

Brenner S (1974) The genetics of Caenorhabditis elegans. *Genetics* 77: 71-94

Chawla DG, Shah RV, Barth ZK, Lee JD, Badecker KE, Naik A, Brewster MM, Salmon TP, Peel N (2016) Caenorhabditis elegans glutamylating enzymes function redundantly in male mating. *Biol Open* 5: 1290-1298

Chen CW, Peng YF, Yen YC, Bhan P, Muthaiyan Shanmugam M, Klopfenstein DR, Wagner OI (2019) Insights on UNC-104-dynein/dynactin interactions and their implications on axonal transport in Caenorhabditis elegans. *J Neurosci Res* 97: 185-201

Chen J, Roll-Mecak A (2023) Glutamylation is a negative regulator of microtubule growth. *Mol Biol Cell* 34: ar70

Citterio A, Arnoldi A, Panzeri E, Merlini L, D'Angelo MG, Musumeci O, Toscano A, Bondi A, Martinuzzi A, Bresolin N *et al* (2015) Variants in KIF1A gene in dominant and sporadic forms of hereditary spastic paraparesis. *Journal of neurology* 262: 2684-2690

Dominguez J, Shah BP, Peel N (2022) A ccpp-6 deletion mutation does not impair gross cilia integrity in C. elegans. *MicroPubl Biol* 2022

Dunn S, Morrison EE, Liverpool TB, Molina-Paris C, Cross RA, Alonso MC, Peckham M (2008) Differential trafficking of Kif5c on tyrosinated and detyrosinated microtubules in live cells. *J Cell Sci* 121: 1085-1095

Ebberink E, Fernandes S, Hatzopoulos G, Agashe N, Chang PH, Guidotti N, Reichart TM, Reymond L, Velluz MC, Schneider F *et al* (2023) Tubulin engineering by semi-synthesis reveals that polyglutamylation directs detyrosination. *Nat Chem* 15: 1179-1187

Erck C, Peris L, Andrieux A, Meissirel C, Gruber AD, Vernet M, Schweitzer A, Saoudi Y, Pointu H, Bosc C *et al* (2005) A vital role of tubulin-tyrosine-ligase for neuronal organization. *Proc Natl Acad Sci U S A* 102: 7853-7858

Eves-van den Akker S, Lilley CJ, Ault JR, Ashcroft AE, Jones JT, Urwin PE (2014) The feeding tube of cyst nematodes: characterisation of protein exclusion. *PLoS One* 9: e87289

Fernandez-Gonzalez A, La Spada AR, Treadaway J, Higdon JC, Harris BS, Sidman RL, Morgan JI, Zuo J (2002) Purkinje cell degeneration (pcd) phenotypes caused by mutations in the axotomy-induced gene, Nna1. *Science* 295: 1904-1906

Genova M, Grycova L, Puttrich V, Magiera MM, Lansky Z, Janke C, Braun M (2023) Tubulin polyglutamylation differentially regulates microtubule-interacting proteins. *EMBO J* 42: e112101

Ghosh-Roy A, Goncharov A, Jin Y, Chisholm AD (2012) Kinesin-13 and tubulin posttranslational modifications regulate microtubule growth in axon regeneration. *Dev Cell* 23: 716-728

Gilmore-Hall S, Kuo J, Ward JM, Zahra R, Morrison RS, Perkins G, La Spada AR (2019) CCP1 promotes mitochondrial fusion and motility to prevent Purkinje cell neuron loss in pcd mice. *J Cell Biol* 218: 206-219

Guardia CM, Farias GG, Jia R, Pu J, Bonifacino JS (2016) BORC Functions Upstream of Kinesins 1 and 3 to Coordinate Regional Movement of Lysosomes along Different Microtubule Tracks. *Cell Rep* 17: 1950-1961

Hall DH, Hedgecock EM (1991) Kinesin-related gene unc-104 is required for axonal transport of synaptic vesicles in C. elegans. *Cell* 65: 837-847

Hamed MB, Vrancken K, Bilyk B, Koepff J, Novakova R, van Mellaert L, Oldiges M, Luzhetskyy A, Kormanec J, Anne J *et al* (2018) Monitoring Protein Secretion in Streptomyces Using Fluorescent Proteins. *Front Microbiol* 9: 3019

Hirokawa N, Niwa S, Tanaka Y (2010) Molecular motors in neurons: transport mechanisms and roles in brain function, development, and disease. *Neuron* 68: 610-638

Hotta T, Plemmons A, Gebbie M, Ziehm TA, Blasius TL, Johnson C, Verhey KJ, Pearring JN, Ohi R (2023) Mechanistic Analysis of CCP1 in Generating DeltaC2 alpha-Tubulin in Mammalian Cells and Photoreceptor Neurons. *Biomolecules* 13

Ikegami K, Heier RL, Taruishi M, Takagi H, Mukai M, Shimma S, Taira S, Hatanaka K, Morone N, Yao I *et al* (2007) Loss of alpha-tubulin polyglutamylation in ROSA22 mice is associated with abnormal targeting of KIF1A and modulated synaptic function. *Proc Natl Acad Sci U S A* 104: 3213-3218

Janke C, Magiera MM (2020) The tubulin code and its role in controlling microtubule properties and functions. *Nat Rev Mol Cell Biol* 21: 307-326

Janke C, Rogowski K, van Dijk J (2008) Polyglutamylation: a fine-regulator of protein function? 'Protein Modifications: beyond the usual suspects' review series. *EMBO Rep* 9: 636-641

Janke C, Rogowski K, Wloga D, Regnard C, Kajava AV, Strub JM, Temurak N, van Dijk J, Boucher D, van Dorsselaer A *et al* (2005) Tubulin polyglutamylase enzymes are members of the TTL domain protein family. *Science* 308: 1758-1762

Kahn OI, Sharma V, Gonzalez-Billault C, Baas PW (2015) Effects of kinesin-5 inhibition on dendritic architecture and microtubule organization. *Mol Biol Cell* 26: 66-77

Kalinina E, Biswas R, Berezniuk I, Hermoso A, Aviles FX, Fricker LD (2007) A novel subfamily of mouse cytosolic carboxypeptidases. *FASEB J* 21: 836-850

Kashiwaya K, Nakagawa H, Hosokawa M, Mochizuki Y, Ueda K, Piao L, Chung S, Hamamoto R, Eguchi H, Ohigashi H *et al* (2010) Involvement of the tubulin tyrosine ligase-like family member 4 polyglutamylase in PELP1 polyglutamylation and chromatin remodeling in pancreatic cancer cells. *Cancer Res* 70: 4024-4033

Kimura S, Noda T, Yoshimori T (2007) Dissection of the autophagosome maturation process by a novel reporter protein, tandem fluorescent-tagged LC3. *Autophagy* 3: 452-460

Kimura Y, Kurabe N, Ikegami K, Tsutsumi K, Konishi Y, Kaplan OI, Kunitomo H, Iino Y, Blacque OE, Setou M (2010) Identification of tubulin deglutamylase among Caenorhabditis elegans and mammalian cytosolic carboxypeptidases (CCPs). *J Biol Chem* 285: 22936-22941

Klimas AS, Dominguez J, Shah BP, Lee ZY, Peel N (2023) The C. elegans deglutamylase CCPP-6 does not operate redundantly with CCPP-1 in gross cilia integrity. *MicroPubl Biol* 2023

Kubo T, Yanagisawa HA, Yagi T, Hirono M, Kamiya R (2010) Tubulin polyglutamylation regulates axonemal motility by modulating activities of inner-arm dyneins. *Curr Biol* 20: 441-445

Lacroix B, van Dijk J, Gold ND, Guizetti J, Aldrian-Herrada G, Rogowski K, Gerlich DW, Janke C (2010) Tubulin polyglutamylation stimulates spastin-mediated microtubule severing. *J Cell Biol* 189: 945-954

Lechtreck KF, Geimer S (2000) Distribution of polyglutamylated tubulin in the flagellar apparatus of green flagellates. *Cell Motil Cytoskeleton* 47: 219-235

Lessard DV, Zinder OJ, Hotta T, Verhey KJ, Ohi R, Berger CL (2019) Polyglutamylation of tubulin's C-terminal tail controls pausing and motility of kinesin-3 family member KIF1A. *J Biol Chem* 294: 6353-6363

Li J, Snyder EY, Tang FHF, Pasqualini R, Arap W, Sidman RL (2020) Nna1 gene deficiency triggers Purkinje neuron death by tubulin hyperglutamylation and ER dysfunction. *JCI Insight* 5

Lu C, Srayko M, Mains PE (2004) The Caenorhabditis elegans microtubule-severing complex MEI-1/MEI-2 katanin interacts differently with two superficially redundant beta-tubulin isotypes. *Mol Biol Cell* 15: 142-150

Lu YM, Zheng C (2022) The Expression and Function of Tubulin Isotypes in Caenorhabditis elegans. *Front Cell Dev Biol* 10: 860065

Magiera MM, Bodakuntla S, Ziak J, Lacomme S, Marques Sousa P, Leboucher S, Hausrat TJ, Bosc C, Andrieux A, Kneussel M *et al* (2018) Excessive tubulin polyglutamylation causes neurodegeneration and perturbs neuronal transport. *EMBO J* 37

Mahalingan KK, Keith Keenan E, Strickland M, Li Y, Liu Y, Ball HL, Tanner ME, Tjandra N, Roll-Mecak A (2020) Structural basis for polyglutamate chain initiation and elongation by TTLL family enzymes. *Nat Struct Mol Biol* 27: 802-813

Matsushita-Ishiodori Y, Yamanaka K, Ogura T (2007) The C. elegans homologue of the spastic paraplegia

protein, spastin, disassembles microtubules. *Biochem Biophys Res Commun* 359: 157-162
Millecamps S, Julien JP (2013) Axonal transport deficits and neurodegenerative diseases. *Nat Rev Neurosci* 14: 161-176
Morikawa M, Jerath NU, Ogawa T, Morikawa M, Tanaka Y, Shy ME, Zuchner S, Hirokawa N (2022) A neuropathy-associated kinesin KIF1A mutation hyper-stabilizes the motor-neck interaction during the ATPase cycle. *Embo j* 41: e108899
Moutin MJ, Bosc C, Peris L, Andrieux A (2021) Tubulin post-translational modifications control neuronal development and functions. *Dev Neurobiol* 81: 253-272
Muniesh MS, Barmaver SN, Huang HY, Bayansan O, Wagner OI (2020) PTP-3 phosphatase promotes intramolecular folding of SYD-2 to inactivate kinesin-3 UNC-104 in neurons. *Mol Biol Cell* 31: 2932-2947
Neumann B, Hilliard MA (2014) Loss of MEC-17 leads to microtubule instability and axonal degeneration. *Cell Rep* 6: 93-103
Nieuwenhuis J, Adamopoulos A, Bleijerveld OB, Mazouzi A, Stickel E, Celie P, Altelaar M, Knipscheer P, Perrakis A, Blomen VA *et al* (2017) Vasohibins encode tubulin detyrosinating activity. *Science* 358: 1453-1456
Nirschl JJ, Magiera MM, Lazarus JE, Janke C, Holzbaur EL (2016) alpha-Tubulin Tyrosination and CLIP-170 Phosphorylation Regulate the Initiation of Dynein-Driven Transport in Neurons. *Cell Rep* 14: 2637-2652
O'Hagan R, Piasecki BP, Silva M, Phirke P, Nguyen KC, Hall DH, Swoboda P, Barr MM (2011) The tubulin deglutamylase CCPP-1 regulates the function and stability of sensory cilia in C. elegans. *Curr Biol* 21: 1685-1694
Orbach R, Howard J (2019) The dynamic and structural properties of axonemal tubulins support the high length stability of cilia. *Nat Commun* 10: 1838
Pagnamenta AT, Heemeryck P, Martin HC, Bosc C, Peris L, Uszynski I, Gory-Faure S, Couly S, Deshpande C, Siddiqui A *et al* (2019) Defective tubulin detyrosination causes structural brain abnormalities with cognitive deficiency in humans and mice. *Hum Mol Genet* 28: 3391-3405
Paschal BM, Obar RA, Vallee RB (1989) Interaction of brain cytoplasmic dynein and MAP2 with a common sequence at the C terminus of tubulin. *Nature* 342: 569-572
Paturle-Lafanechere L, Manier M, Trigault N, Pirollet F, Mazarguil H, Job D (1994) Accumulation of delta 2-tubulin, a major tubulin variant that cannot be tyrosinated, in neuronal tissues and in stable microtubule assemblies. *J Cell Sci* 107 (Pt 6): 1529-1543
Ping Y, Ohata K, Kikushima K, Sakamoto T, Islam A, Xu L, Zhang H, Chen B, Yan J, Eto F *et al* (2023) Tubulin Polyglutamylation by TTLL1 and TTLL7 Regulate Glutamate Concentration in the Mice Brain. *Biomolecules* 13
Rogowski K, van Dijk J, Magiera MM, Bosc C, Deloulme JC, Bosson A, Peris L, Gold ND, Lacroix B, Bosch Grau M *et al* (2010) A family of protein-deglutamylating enzymes associated with neurodegeneration. *Cell* 143: 564-578
Romaniello R, Arrigoni F, Bassi MT, Borgatti R (2015) Mutations in alpha- and beta-tubulin encoding genes: implications in brain malformations. *Brain Dev* 37: 273-280
Sanyal C, Pietsch N, Ramirez Rios S, Peris L, Carrier L, Moutin MJ (2023) The detyrosination/re-tyrosination cycle of tubulin and its role and dysfunction in neurons and cardiomyocytes. *Semin Cell Dev Biol* 137: 46-

62
Schneider CA, Rasband WS, Eliceiri KW (2012) NIH Image to ImageJ: 25 years of image analysis. *Nat Methods* 9: 671-675
Siddiqui N, Straube A (2017) Intracellular Cargo Transport by Kinesin-3 Motors. *Biochemistry (Mosc)* 82: 803-815
Soppina V, Verhey KJ (2014) The family-specific K-loop influences the microtubule on-rate but not the superprocessivity of kinesin-3 motors. *Mol Biol Cell* 25: 2161-2170
Suryavanshi S, Edde B, Fox LA, Guerrero S, Hard R, Hennessey T, Kabi A, Malison D, Pennock D, Sale WS *et al* (2010) Tubulin glutamylation regulates ciliary motility by altering inner dynein arm activity. *Curr Biol* 20: 435-440
Szczesna E, Zehr EA, Cummings SW, Szyk A, Mahalingan KK, Li Y, Roll-Mecak A (2022) Combinatorial and antagonistic effects of tubulin glutamylation and glycylation on katanin microtubule severing. *Dev Cell* 57: 2497-2513 e2496
Tas RP, Chazeau A, Cloin BMC, Lambers MLA, Hoogenraad CC, Kapitein LC (2017) Differentiation between Oppositely Oriented Microtubules Controls Polarized Neuronal Transport. *Neuron* 96: 1264-1271 e1265
Tien NW, Wu GH, Hsu CC, Chang CY, Wagner OI (2011) Tau/PTL-1 associates with kinesin-3 KIF1A/UNC-104 and affects the motor's motility characteristics in C. elegans neurons. *Neurobiol Dis* 43: 495-506
Valenstein ML, Roll-Mecak A (2016) Graded Control of Microtubule Severing by Tubulin Glutamylation. *Cell* 164: 911-921
van der Vaart B, Akhmanova A, Straube A (2009) Regulation of microtubule dynamic instability. *Biochem Soc Trans* 37: 1007-1013
van Dijk J, Rogowski K, Miro J, Lacroix B, Edde B, Janke C (2007) A targeted multienzyme mechanism for selective microtubule polyglutamylation. *Mol Cell* 26: 437-448
Wagner OI, Esposito A, Kohler B, Chen CW, Shen CP, Wu GH, Butkevich E, Mandalapu S, Wenzel D, Wouters FS *et al* (2009) Synaptic scaffolding protein SYD-2 clusters and activates kinesin-3 UNC-104 in C. elegans. *Proc Natl Acad Sci U S A* 106: 19605-19610
Wang X, Song K, Li Y, Tang L, Deng X (2019) Single-Molecule Imaging and Computational Microscopy Approaches Clarify the Mechanism of the Dimerization and Membrane Interactions of Green Fluorescent Protein. *Int J Mol Sci* 20
Ward S, Burke DJ, Sulston JE, Coulson AR, Albertson DG, Ammons D, Klass M, Hogan E (1988) Genomic organization of major sperm protein genes and pseudogenes in the nematode Caenorhabditis elegans. *J Mol Biol* 199: 1-13
Westermann S, Weber K (2003) Post-translational modifications regulate microtubule function. *Nat Rev Mol Cell Biol* 4: 938-947
Wloga D, Rogowski K, Sharma N, Van Dijk J, Janke C, Edde B, Bre MH, Levilliers N, Redeker V, Duan J *et al* (2008) Glutamylation on alpha-tubulin is not essential but affects the assembly and functions of a subset of microtubules in Tetrahymena thermophila. *Eukaryot Cell* 7: 1362-1372
Wu GH, Muthaiyan Shanmugam M, Bhan P, Huang YH, Wagner OI (2016) Identification and Characterization of LIN-2(CASK) as a Regulator of Kinesin-3 UNC-104(KIF1A) Motility and Clustering in Neurons. *Traffic* 17: 891-907

Wu HY, Rong Y, Correia K, Min J, Morgan JI (2015) Comparison of the enzymatic and functional properties of three cytosolic carboxypeptidase family members. *J Biol Chem* 290: 1222-1232

Yonekawa Y, Harada A, Okada Y, Funakoshi T, Kanai Y, Takei Y, Terada S, Noda T, Hirokawa N (1998) Defect in synaptic vesicle precursor transport and neuronal cell death in KIF1A motor protein-deficient mice. *J Cell Biol* 141: 431-441

Zaniewski TM, Hancock WO (2023) Positive charge in the K-loop of the kinesin-3 motor KIF1A regulates superprocessivity by enhancing microtubule affinity in the one-head-bound state. *J Biol Chem* 299: 102818